

Novel Collective Excitations and Quasi-particle Picture of Quarks Coupled with a Massive Boson at Finite Temperature

Masakiyo KITAZAWA^{ab*)} Teiji KUNIHIRO^{a**)} and Yukio NEMOTO^{c***)}

^a *Yukawa Institute for Theoretical Physics, Kyoto University, Kyoto, 606-8502, Japan*

^b *RIKEN-BNL Research Center, Brookhaven National Laboratory, Upton, NY 11973, USA*

^c *Department of Physics, Nagoya University, Naoya, 464-8602, Japan*

Motivated by the observation that there may exist hadronic excitations even in the quark-gluon plasma (QGP) phase, we investigate how the quark properties, especially its possible quasi-particle picture, are affected by the coupling with bosonic excitations at finite temperature(T), employing Yukawa models with a massive scalar (pseudoscalar) and vector (axial-vector) boson with a mass m . The quark spectral function and the quasi-dispersion relations are calculated at the one-loop order. We find that there appears a three-peak structure in the quark spectral function with a collective nature when T is comparable with m , irrespective of the type of the boson; such a multi-peak structure was first found in a chiral model yielding scalar composite bosons with a decay width. We elucidate the mechanism of realizing the new quark collective excitations in terms of the Landau damping of a quark (an antiquark) induced by the scattering with the thermally excited boson, which gives rise to a mixing and hence a level repulsion between a quark (antiquark) and an antiquark-hole (quark-hole) in the thermally excited antiquark(quark) distribution. Our results suggest that the quarks in the QGP phase may have an interesting quasi-particle picture with a multi-peak spectral function. Since the used models are rather generic, our findings may be a universal phenomenon for fermions coupled to a massive bosonic excitation with a vanishing or small width. Relevance of the results to other fields of physics, such as neutrino physics, is also briefly mentioned. We also give a new aspect of the plasmino excitation obtained in the hard-thermal loop approximation.

§1. Introduction

The exploration of phase transitions in quantum chromodynamics (QCD) and the examination of the nature of the new form of the QCD matter in extreme conditions such as high temperature (T) and density are of great interest. One of the central issues in this field is revealing the physical contents of the so called quark-gluon plasma (QGP) phase. Although it was widely believed for a long time that the QGP phase even just after the deconfinement transition is composed of weakly interacting quarks and gluons in accordance with the asymptotic freedom of QCD, such a view is now taken to be too naive. In fact, it has been being elucidated experimentally and theoretically that the QGP phase near the critical point of the chiral and deconfinement phase transitions, has a non-trivial structure since the strong coupling nature of QCD really comes to play. The experiments at Relativistic Heavy

^{*)} kitazawa@quark.phy.bnl.gov

^{**)} kunihiro@yukawa.kyoto-u.ac.jp

^{***)} nemoto@hken.phys.nagoya-u.ac.jp

Ion Collider (RHIC) at BNL are accessible to the QGP phase near the critical temperature (T_c) of the deconfinement and the chiral phase transitions. It is argued¹⁾ that the experimental results at RHIC suggest that the created matter behaves like a perfect fluid, which implies that the QGP near T_c is a strongly coupled system and may be called the sQGP where the “s” stands for “strongly coupled”. This suggestion seems to be consistent with the recent lattice QCD simulations²⁾ showing that the charmonium states survive at higher temperature above T_c of the deconfinement transition than originally expected.³⁾ The existence of hadronic excitations in the light quark sector in the QGP phase was also suggested even before on the basis of the symmetry nature of the chiral transition^{4)*}, where it was argued and demonstrated using a chiral effective model that if the chiral transition is a second order or nearly second order, there may exist the soft modes of the phase transition above T_c , which have the same quantum numbers as those of the sigma meson and the pion.

Now the quarks and the gluons are the basic degrees of freedom in the QGP phase, so it must be of basic importance to clarify the properties of them even apart from possible hadronic excitations. In fact, the success of the recombination (or coalescence) model⁶⁾ for account for the quark-number scaling of the so called v_2 parameter of the collective flow seen in RHIC experiments strongly suggests that there exist quasi-particles with quark quantum numbers in the matter created at RHIC. Therefore it is imperative^{7),8)} to clarify how the strong coupling nature of the sQGP and the quark quasi-particle picture can be compatible. The present work is concerned with the quark properties in a strong coupling system at finite T .

It is remarkable that even in the high- T limit where the hard thermal loop (HTL) approximation⁹⁾ is established, the quarks have some collective nature,¹⁰⁾ as the gluons become the plasmons:^{11),12)} The quarks have two branches of spectrum, i.e., the normal quasi-quark and the plasmino,¹³⁾ the latter of which does not exist at zero T and density. The origin of the formation of the plasmino excitation at high T is discussed in Ref. 14) **), where it is shown that the appearance of the plasmino at high T is owing to the fact that hole states of thermally excited particles as well as anti-particles can be created.

In the vicinity of T_c of the chiral phase transition, the non-perturbative effects are important, and one may expect, on the general ground, that the quarks will show a novel and complicated properties.^{7),16)} In a previous work,⁷⁾ the present authors explored the quark spectrum near but above T_c of the chiral transition, focusing on the effects of the chiral soft modes.⁴⁾ A surprise was that the quasi-quarks and quasi-antiquarks acquire a novel collective nature owing to the coupling of the quarks with the soft modes so that the quark spectral function gets to have a *three-peak* structure, as T approaches T_c .⁷⁾ What makes the three-peak structure in the fermion spectrum? In reality, the soft modes correspond to a pronounced peak in the time-like region with a width in the spectral function in a bosonic channel: The peak position at the

^{*)} See also Ref. 5) in which a quite different reasoning is given for the possibility of the color-singlet excitations in the QGP phase.

^{**) The origin of a similar spectrum at zero T but high density is discussed in Ref. 15).}

momentum \mathbf{p} can be expressed approximately as $\omega \simeq \pm\sqrt{m_\sigma^*(T)^2 + |\mathbf{p}|^2}$ with a T -dependent ‘mass’ $m_\sigma^*(T)$, and as T approaches T_c , $m_\sigma^*(T)$ becomes smaller together with the width of the peaks. It means that whenever the multi-peak structure of the quark spectral function shows up, the soft modes have the character of a well-defined elementary boson with a mass, which is found to be comparable with T^7) $^*)$. Thus one sees that a smaller width of the bosonic excitation is favorable for the multi-peak spectral function, and expects that a system composed of a (massless) quark and an elementary massive boson as described by a Yukawa model may exhibit the multi-peak structure in the quark spectral function.

In this paper, we examine quantitatively the quark properties at finite T using Yukawa models with a massive boson coupled to a massless quark. We consider two types of bosons, i.e., massive scalar (pseudoscalar) and vector (axial-vector) bosons with a mass m ; notice that since the quark is massless, the scalar (vector) and pseudoscalar (axial-vector) give the same results in the perturbation theory. We calculate the spectral function and the quasi-dispersion relation of the quark at finite T at the one-loop order. We show that a three-peak structure in the quark spectral function is formed when $T \sim m$, irrespective of the boson types. We elucidate the mechanism of realizing the new quark collective excitations in terms of the Landau damping of a quark (an antiquark) induced by the scattering with the thermally excited boson, which gives rise to a mixing and hence a level repulsion between a quark (antiquark) and an antiquark-hole (quark-hole) in the thermally excited quark (antiquark) distribution; such a mechanism of the particle mixing is called a “resonant scattering”. $^{7),19),20)$ We shall also show that the high- T and weak-coupling limit of the fermion spectrum approaches the one in the HTL approximation, and thereby show that the plasmino excitation obtained in the HTL approximation can be understood to be originated from a level repulsion between a collective quark and an anti-quark excitations.

Our results suggest that the quarks in the QGP phase may have an interesting quasi-particle picture with a multi-peak spectral function, since there may exist bosonic excitations in the QGP phase. Furthermore, seeing that the models employed here are rather generic, one may expect that the appearance of the novel three-peak structure in the fermion spectrum may be a universal phenomenon for fermions coupled to a bosonic excitation with a vanishing or small width irrespective of the type of the bosonic excitation.

This paper is organized as follows. In Sec. 2, the spectral function and the (quasi)-dispersion relation of the fermion, which are frequently used in the following sections, are summarized. We emphasize that the quasi-dispersion relations may not describe the physical excitations when the imaginary part of the quark self-energy

$^*)$ The bosonic excitation corresponding to a peak of the spectral function in the time-like region with a small width is a propagating mode with a small damping effect. Such a mode is in contrast to those in the (color-)super-conducting transition, which is almost diffusive with a strength concentrated around the Fermi surface. $^{17),18)$ Through a coupling with the diffusive soft mode, the quark spectrum can form a *two-peak* structure, $^{19)}$ which brings about the pseudogap in the density of states of quarks. $^{16),17)$ Thus one sees that the difference of the number of the peaks in the quark spectral function comes from that of the nature of the respective soft modes.

is large. In Sec. 3, we investigate the fermion spectrum in a Yukawa model with a massive scalar boson. We show that a three-peak structure in the fermion spectral function is formed when $T \sim m$. We clarify the mechanism for realizing the multi-peak structure in the spectral function in terms of the Landau damping and the resonant scattering. The high- T and weak-coupling limit of the fermion spectrum is also discussed. In Sec. 4, we examine the fermion spectrum in a Yukawa model with a massive vector boson. We shall see that the appearance of the three-peak structure in the fermion spectral function occurs irrespective of the type of the boson. The relevance of the result to the QGP physics is briefly mentioned. The last section is devoted to a brief summary and concluding remarks. In Appendices, some technical details of the calculations of the formulae given in the text are presented.

§2. Generalities about quark spectral function and dispersion relations at finite temperature

In this section, we summarize general features of the spectral function and the quasi-dispersion relations of the Dirac fermion, which we call a ‘quark’, at finite T . Although the contents of this section may be familiar to the readers, this section serves the introduction of the notations to be used in the subsequent sections.

The quark spectral function $\mathcal{A}(\mathbf{p}, \omega)$ is expressed as¹⁷⁾

$$\mathcal{A}(\mathbf{p}, \omega) = -\frac{1}{\pi} \cdot \text{Im}G^R(\mathbf{p}, \omega) \equiv -\frac{1}{\pi} \frac{G^R(\mathbf{p}, \omega) - \gamma^0 G^{R\dagger}(\mathbf{p}, \omega) \gamma^0}{2i}, \quad (2.1)$$

where $G^R(\mathbf{p}, \omega)$ is the retarded Green functions of the quark,

$$G^R(\mathbf{p}, \omega) = \frac{1}{(\omega + i\eta)\gamma^0 - \mathbf{p} \cdot \boldsymbol{\gamma} + m_f - \Sigma^R(\mathbf{p}, \omega)}, \quad (2.2)$$

with the quark mass m_f and the retarded self-energy $\Sigma^R(\mathbf{p}, \omega)$. The spectral function $\mathcal{A}(\mathbf{p}, \omega)$ has the same matrix structure as the Green function. Because of the absence of the Lorentz invariance at finite T , $\mathcal{A}(\mathbf{p}, \omega)$ generically has the following Dirac structure

$$\mathcal{A}(\mathbf{p}, \omega) = \rho_0(\mathbf{p}, \omega)\gamma^0 - \rho_v(\mathbf{p}, \omega)\hat{\mathbf{p}} \cdot \boldsymbol{\gamma} + \rho_s(\mathbf{p}, \omega), \quad (2.3)$$

where $\hat{\mathbf{p}} = \mathbf{p}/|\mathbf{p}|$ and we have assumed the rotational and the parity invariances. The temporal part $\rho_0(\mathbf{p}, \omega)$ represents the quark number excitations of the system.

When $m_f = 0$ and $\text{Tr}\Sigma^R = 0$ with Tr denoting the trace over the Dirac index, the chiral symmetry is hold and $\rho_s(\mathbf{p}, \omega)$ vanishes. In this case, the self-energy is written as $\Sigma^R = \Sigma_0\gamma^0 - \Sigma_v\boldsymbol{\gamma} \cdot \hat{\mathbf{p}}$ and the Green function eq. (2.2) is decomposed using the projection operators $\Lambda_{\pm}(\mathbf{p}) = (1 \pm \gamma^0\hat{\mathbf{p}} \cdot \boldsymbol{\gamma})/2$ as

$$G^R(\mathbf{p}, \omega) = G_+(\mathbf{p}, \omega)\Lambda_+(\mathbf{p})\gamma^0 + G_-(\mathbf{p}, \omega)\Lambda_-(\mathbf{p})\gamma^0, \quad (2.4)$$

with

$$G_{\pm}(\mathbf{p}, \omega) = \frac{1}{2} \text{Tr}[G^R\gamma^0\Lambda_{\pm}(\mathbf{p})] = \frac{1}{\omega + i\eta \mp |\mathbf{p}| - \Sigma_{\pm}(\mathbf{p}, \omega)}, \quad (2.5)$$

and $\Sigma_{\pm}(\mathbf{p}, \omega) = (1/2)\text{Tr}[\Sigma^R \Lambda_{\pm}(\mathbf{p}) \gamma^0] = \Sigma_0 \mp \Sigma_v$. The spectral function $\mathcal{A}(\mathbf{p}, \omega)$ is also written as

$$\mathcal{A}(\mathbf{p}, \omega) = \rho_+(\mathbf{p}, \omega) \Lambda_+(\mathbf{p}) \gamma^0 + \rho_-(\mathbf{p}, \omega) \Lambda_-(\mathbf{p}) \gamma^0, \quad (2.6)$$

where

$$\rho_{\pm}(\mathbf{p}, \omega) = -\frac{1}{\pi} \text{Im} G_{\pm} = \rho_0(\mathbf{p}, \omega) \mp \rho_v(\mathbf{p}, \omega) \quad (2.7)$$

represents the spectrum of the quark and the anti-quark excitations. Note that Σ_{\pm} , G_{\pm} and ρ_{\pm} are scalar functions, while Σ^R , G^R and ρ are matrices in the Dirac space. In the non-interacting system, we have the spectral function of the massless quark proportional to the delta function, $\rho_{\pm}^{\text{free}}(\mathbf{p}, \omega) = \delta(\omega \mp |\mathbf{p}|)$. At zero density, $\rho_+(\mathbf{p}, \omega)$ and $\rho_-(\mathbf{p}, \omega)$ have a simple symmetric property owing to the charge conjugation invariance,

$$\rho_+(\mathbf{p}, \omega) = \rho_-(\mathbf{p}, -\omega). \quad (2.8)$$

Poles of $G_{\pm}(\mathbf{p}, \omega)$, $z = z_{\pm}(\mathbf{p})$, represent collective excitations of the quark and the antiquark sectors, respectively. They are obtained by solving the equations

$$z_{\pm}(\mathbf{p}) \mp |\mathbf{p}| - \Sigma_{\pm}(\mathbf{p}, z_{\pm}(\mathbf{p})) = 0, \quad (2.9)$$

in the complex energy-plane. The retarded self-energy assures that the solutions z_{\pm} lie in the lower-half plane owing to the causality. Equation (2.9) may have several solutions for fixed momentum $|\mathbf{p}|$, and $\rho_{\pm}(\mathbf{p}, \omega)$ may have multi-peak structure associated with these poles.

For convenience, we also define the quasi-dispersion relations $\omega = \omega_{\pm}(\mathbf{p})$ as the zero of the *real part* of the inverse Green functions;

$$\omega_{\pm}(\mathbf{p}) \mp |\mathbf{p}| = \text{Re} \Sigma_{\pm}(\mathbf{p}, \omega_{\pm}(\mathbf{p})). \quad (2.10)$$

Solving eq. (2.10) is much easier than that of eq. (2.9) in the complex plane. The functions $\omega_{\pm}(\mathbf{p})$ are real numbers and eq. (2.10) may have several solutions for fixed \mathbf{p} . When the condition $\text{Im} \Sigma_{\pm}(\mathbf{p}, \omega_{\pm}(\mathbf{p})) \ll \omega_{\pm}(\mathbf{p})$ is satisfied and hence the quasi-particle picture in the Landau's sense is valid, the difference between $\text{Re} z_{\pm}$ and ω_{\pm} is small, then $\omega_{\pm}(\mathbf{p})$ is approximately regarded as the excitation energy of the quasi-particles and can be used as an eye-guide of positions of the peak in ρ_{\pm} ^{*)}. We shall often use the quasi-dispersion relations in the rest of the paper.

§3. Quark spectrum in a Yukawa model with a massive scalar (pseudoscalar) boson

In this section, we investigate the spectrum of a massless quark ψ in a Yukawa model with a massive scalar (pseudoscalar) boson ϕ at finite T . A detailed analysis

^{*)} In this sense, when this condition is satisfied, peaks of the spectral function and the quasi-dispersion relation, which are gauge-dependent in the gauge theories, well reflect the position of the gauge-independent poles of the Green function.

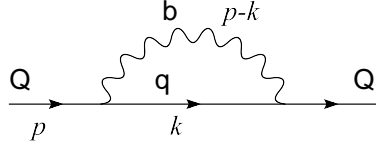


Fig. 1. The quark self-energy at the one-loop order.

of a *massive quark* coupled with a *massless boson* at vanishing momentum was made in Ref. 21). As we will see, the finite boson mass gives rise to an unexpectedly interesting complications to the quark spectrum, which were not seen in Ref. 21).

We start from the following Lagrangian composed of a quark and a scalar boson;

$$\mathcal{L} = \bar{\psi}(i\partial - g\phi)\psi + \frac{1}{2}(\partial_\mu\phi\partial^\mu\phi - m^2\phi^2), \quad (3.1)$$

with the coupling constant g and the boson mass m . We notice that the if the boson is pseudoscalar, g should be replaced with $i\gamma_5 g$. As we shall see, however, this replacement does not lead any difference in the results for the quark spectrum.

3.1. Quark self-energy

3.1.1. Formulation

The quark self-energy in the imaginary time formalism at the one-loop order, shown in Fig. 1, is expressed as

$$\tilde{\Sigma}(\mathbf{p}, i\omega_m) = -g^2 T \sum_n \int \frac{d^3\mathbf{k}}{(2\pi)^3} \mathcal{G}_0(\mathbf{k}, i\omega_n) \mathcal{D}(\mathbf{p} - \mathbf{k}, i\omega_m - i\omega_n) \quad (3.2)$$

where $\mathcal{G}_0(\mathbf{k}, i\omega_n) = [i\omega_n \gamma^0 - \mathbf{k} \cdot \boldsymbol{\gamma}]^{-1}$ and $\mathcal{D}(\mathbf{k}, i\nu_n) = [(i\nu_n)^2 - \mathbf{k}^2 - m^2]^{-1}$ are the Matsubara Green functions for the free quark and scalar boson, respectively, and $i\omega_n = (2n + 1)\pi T$ and $i\nu_n = 2n\pi T$ are the Matsubara frequencies for the fermion and boson, respectively.

For the coupling with a pseudoscalar boson, a factor $i\gamma_5$ is added in both sides of \mathcal{G}_0 in eq. (3.2). Such a factor is, however, canceled out because it anti-commutes with \mathcal{G}_0 and thus the self-energy becomes the same form as eq (3.2). Therefore, the following results and discussion in this section hold also for the coupling with a pseudoscalar boson, as mentioned before.

In accordance with the standard procedure in the imaginary time formalism, we take the summation of the Matsubara modes n and the analytic continuation $i\omega_m \rightarrow \omega + i\eta$ (see Appendix A for the detail). The result is given by

$$\begin{aligned} \Sigma^R(\mathbf{p}, \omega) = g^2 \int \frac{d^3\mathbf{k}}{(2\pi)^3} \frac{1}{2E_b} & \left\{ \Lambda_+(\mathbf{k}) \frac{1 + n(E_b) - f(E_f)}{\omega - E_f - E_b + i\eta} + \Lambda_-(\mathbf{k}) \frac{n(E_b) + f(E_f)}{\omega + E_f - E_b + i\eta} \right. \\ & \left. + \Lambda_+(\mathbf{k}) \frac{n(E_b) + f(E_f)}{\omega - E_f + E_b + i\eta} + \Lambda_-(\mathbf{k}) \frac{1 + n(E_b) - f(E_f)}{\omega + E_f + E_b + i\eta} \right\} \gamma^0, \end{aligned} \quad (3.3)$$

where $E_f = |\mathbf{k}|$, $E_b = \sqrt{(\mathbf{p} - \mathbf{k})^2 + m^2}$, and $n(E) = [\exp(E/T) - 1]^{-1}$ and $f(E) = [\exp(E/T) + 1]^{-1}$ are the Bose-Einstein and the Fermi-Dirac distribution functions, respectively.

The self-energy eq. (3.3) has an ultraviolet divergence which comes from the T -independent part $\Sigma^R(\mathbf{p}, \omega)_{T=0} \equiv \lim_{T \rightarrow 0} \Sigma^R(\mathbf{p}, \omega)$. To eliminate the divergence, we renormalize this part by imposing the on-shell renormalization condition. See Appendix C for the detail of the renormalization procedure. The renormalized self-energy is written as

$$\Sigma^R(\mathbf{p}, \omega)_{T=0} = \frac{g^2 \not{p}}{32\pi^2} \left\{ \left(1 - \frac{m^2}{P^2}\right)^2 \ln \frac{P^2 - m^2}{m^2} - \frac{3}{2} + \frac{m^2}{P^2} \right\}, \quad (3.4)$$

with $p_\mu = (\omega, \mathbf{p})$ and $P^2 = p_\mu p^\mu$. Notice that there is no infrared divergence in eq. (3.3) as long as the scalar boson is massive. Since the T -dependent ($T \neq 0$) part $\Sigma^R(\mathbf{p}, \omega)_{T \neq 0} \equiv \Sigma^R(\mathbf{p}, \omega) - \Sigma^R(\mathbf{p}, \omega)_{T=0}$ does not have any divergences, we can evaluate it without any regularization (see Appendix A). For the numerical calculations of the $T \neq 0$ part, it is convenient to first derive the imaginary part $\text{Im}\Sigma^R(\mathbf{p}, \omega)_{T \neq 0}$, and then determine the real part using the dispersion (Kramers-Kronig) relation

$$\text{Re}\Sigma^R(\mathbf{p}, \omega)_{T \neq 0} = -\frac{1}{\pi} P \int_{-\infty}^{\infty} d\omega' \frac{\text{Im}\Sigma^R(\mathbf{p}, \omega')_{T \neq 0}}{\omega - \omega'}. \quad (3.5)$$

The imaginary part of the self-energy $\text{Im}\Sigma^R(\mathbf{p}, \omega)$ is given by

$$\begin{aligned} \text{Im}\Sigma^R(\mathbf{p}, \omega) &= -\pi g^2 \int \frac{d^3 k}{(2\pi)^3} \frac{1}{2E_b} \\ &\times \left\{ \Lambda_+(\mathbf{k})(1+n-f)\delta(\omega - E_f - E_b) \quad (\text{I}) \right. \\ &+ \Lambda_-(\mathbf{k})(n+f)\delta(\omega + E_f - E_b) \quad (\text{II}) \\ &+ \Lambda_+(\mathbf{k})(n+f)\delta(\omega - E_f + E_b) \quad (\text{III}) \\ &\left. + \Lambda_-(\mathbf{k})(1+n-f)\delta(\omega + E_f + E_b) \right\} \gamma^0 \quad (\text{IV}). \end{aligned} \quad (3.6)$$

with $f = f(E_f)$ and $n = n(E_b)$. Each term in eq. (3.6) denoted by (I)-(IV) describes a definite decay process and has a support in the region shown in Fig. 2; the detail of the physical meaning of each term will be discussed in the following.

Let us denote the external quark as Q and the internal one as q as shown in Fig. 1. The former is the quasi-quark interacting with scalar bosons, while the latter is a free quark in the approximation used here. The physical meaning of each term in eq. (3.6) is more transparent when one rewrites eq. (3.6) in terms of the transition probabilities.²²⁾ We can express Σ_+ defined in Sec.2 as

$$\Sigma_+(\mathbf{p}, \omega) = \bar{u}(p) \Sigma^R(\mathbf{p}, \omega) u(p) \quad (3.7)$$

where $u(p)$ is a free quark spinor with the effective mass parameter $\sqrt{P^2}$ which satisfies $(\not{p} - \sqrt{P^2})u(p) = 0$ with the normalization $\bar{u}(p)u(p) = 2\sqrt{P^2}$. We have

$$\text{Im}\Sigma_+(\mathbf{p}, \omega) = -\frac{1}{2} \int \frac{d^3 k_f}{(2\pi)^3} \frac{d^3 k_b}{(2\pi)^3} \frac{1}{2E_f 2E_b} \sum_s (2\pi)^4$$

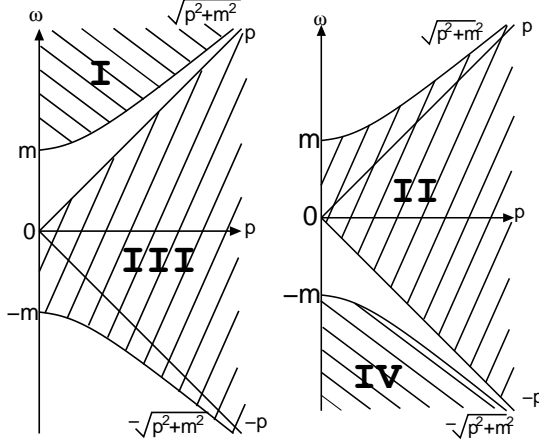


Fig. 2. The supports of the terms (I)-(IV) in eq. (3.6).

$$\begin{aligned}
& \times \left\{ [\delta^4(p - k_f - k_b)|M(Q \rightarrow q, b)|^2[(1-f)(1-n) + fn] \quad (I) \right. \\
& + [\delta^4(p + k_f - k_b)|M(Q, \bar{q} \rightarrow b)|^2[f(1+n) + n(1-f)] \quad (II) \\
& + [\delta^4(p - k_f + k_b)|M(Q, b \rightarrow q)|^2[n(1-f) + f(1+n)] \quad (III) \\
& \left. + [\delta^4(p + k_f + k_b)|M(Q, \bar{q}, b \rightarrow 0)|^2[fn + (1-f)(1-n)]] \right\} \quad (IV), \\
\end{aligned} \tag{3.8}$$

where s is the spin of the quark q and $k_f = (E_f, \mathbf{k})$, $k_b = (E_b, \mathbf{p} - \mathbf{k})$. The amplitudes M are given by

$$\begin{aligned}
M(Q \rightarrow q, b) &= M(Q, b \rightarrow q) = g\bar{u}(p)u(p), \\
M(Q, \bar{q} \rightarrow b) &= M(Q, \bar{q}, b \rightarrow 0) = g\bar{v}(p)u(p),
\end{aligned} \tag{3.9}$$

where $v(p)$ is defined through $(\not{p} + \sqrt{P^2})v(p) = 0$ with the normalization $\bar{v}(p)v(p) = -2\sqrt{P^2}$. The first term in eq. (3.8) with the statistical factor $(1-f)(1+n)$ describes a decay process $Q \rightarrow q + b$ and that with the factor fn describes the inverse one $q + b \rightarrow Q$. The second term with the factor $f(1+n)$ describes $Q + \bar{q} \rightarrow b$ and that with the factor $n(1-f)$ describes $b \rightarrow Q + \bar{q}$. The third and the fourth terms are likewise. These processes are schematically shown in Fig. 3. The terms (II) and (III), which involve a thermally excited particle as an incident particle, vanish as $T \rightarrow 0$ and are known as the Landau damping. They play an important role for the structure of the quark spectral function at finite T , as we will see later.

Similarly, it can be shown that the quantity $\Sigma_-(\mathbf{p}, \omega) = \bar{v}(p)\Sigma^R(\mathbf{p}, \omega)v(p)$ contains amplitudes for the processes, $M(\bar{Q} \rightarrow \bar{q}, b)$, $M(\bar{Q}, q \rightarrow b)$, $M(\bar{Q}, b \rightarrow \bar{q})$, and $M(\bar{Q}, q, b \rightarrow 0)$.

After some manipulations as given in Appendix A, we arrive at the following

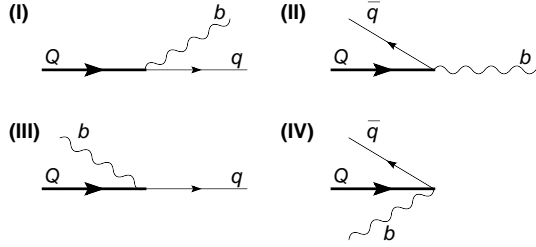


Fig. 3. The kinetic processes contained in $\text{Im}\Sigma_+(\mathbf{p}, \omega)$; the corresponding inverse ones are not shown. The thick solid line Q represents the quasi-quark, the thin solid lines q on-shell free quarks and the wavy lines b the on-shell scalar boson. The incident on-shell particles are thermally excited particles.

result,

$$\begin{aligned} \text{Im}\Sigma_{\pm}(\mathbf{p}, \omega) = & -\frac{g^2}{32\pi p^2} \int_{E_f^+}^{E_f^-} dk [2|\mathbf{p}|E_f \mp (\mathbf{p}^2 + m^2 - \omega^2 + 2\omega E_f)] \\ & \times [1 + n(\omega - E_f) - f(E_f)] \\ & -\frac{g^2}{32\pi p^2} [(|\mathbf{p}| \mp \omega)(\pi^2 T^2 \pm \omega^2) \pm \omega m^2] \theta(\mathbf{p}^2 - \omega^2), \end{aligned} \quad (3.10)$$

with $E_f^{\pm} = (\omega^2 - \mathbf{p}^2 - m^2)/2(\omega \pm |\mathbf{p}|)$. For the vanishing momentum, $\text{Im}\Sigma_+ = \text{Im}\Sigma_-$ and $\text{Im}\Sigma^R$ is simply written as

$$\text{Im}\Sigma^R(\mathbf{p} = 0, \omega) = -\gamma^0 \frac{g^2}{32\pi} \frac{(\omega^2 - m^2)^2}{\omega^3} [n(\omega_b) + f(\omega_q)] \quad (3.11)$$

with

$$\omega_b = \frac{\omega^2 + m^2}{2\omega}, \quad \omega_q = -\frac{\omega^2 - m^2}{2\omega}. \quad (3.12)$$

3.1.2. Numerical results

In the upper panel of Fig. 4, we show $\text{Im}\Sigma_+(\mathbf{p}, \omega)/g^2$, which is independent of g , for the vanishing momentum and several temperatures. We see that $\text{Im}\Sigma_+(\mathbf{0}, \omega)/g^2$ vanishes at $\omega = 0, \pm m$, irrespective of T . These values of ω are located in the boundaries of the regions (I)-(IV) shown in Fig. 2. The vanishing decay rate at $\omega = \pm m$ is owing to the suppression of the phase space; the energy-momentum conservation requires the zero momentum of the on-shell (anti)quark for each process at $\omega = \pm m$. Around $\omega = 0$, on the other hand, the distribution functions in eq. (3.11) suppress the decay rate, because the on-shell energies of the boson and the quark, $|\omega_b|$ and $|\omega_q|$, go to infinity as $\omega \rightarrow 0$.

From Fig. 4, we see that $\text{Im}\Sigma_+(\mathbf{p}, \omega)$ takes finite values only for $|\omega|/m > 1$ at $T = 0$; the corresponding decay processes are represented by (I) and (IV) in Fig. 3. At finite T , the Landau damping comes to play and $\text{Im}\Sigma_+(\mathbf{p}, \omega)$ has a support in the regions (II) and (III) in Fig. 2; the two peaks in these regions grow rapidly as T is raised, and around $T \simeq m$, the Landau damping gets to dominate over the decay rates owing to the processes (I) and (IV) in the energy range shown in Fig. 4.

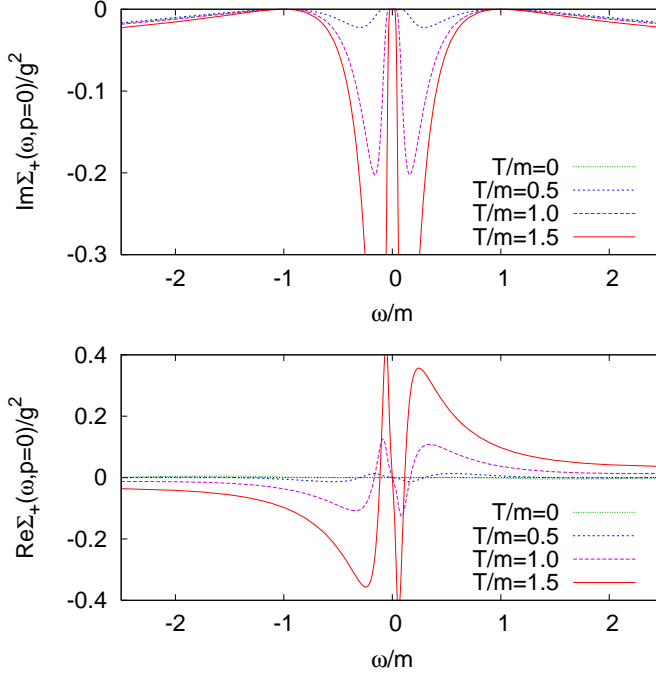


Fig. 4. The imaginary and real parts of the self-energy $\Sigma_+(\mathbf{p}, \omega)$ at zero momentum and several temperatures.

Using the dispersion relation eq. (3.5), we can understand the qualitative behavior of $\text{Re}\Sigma_+(\mathbf{p}, \omega)$ from that of the imaginary part: If there is a sharp peak in the imaginary part, the real part has a steep rise at the same energy. In order to see this relation, we show $\text{Re}\Sigma_+(\mathbf{p}, \omega)/g^2$ for $\mathbf{p} = 0$ in the lower panel of Fig. 4. One sees that there appears oscillating behavior around $\omega = 0$ and the amplitude of the oscillation grows rapidly as T becomes larger, along with the growth of the peaks in $\text{Im}\Sigma_+(\mathbf{p}, \omega)$.

The other important property of $\Sigma_+(\mathbf{p}, \omega)$ shown in Fig. 4 is that both $\text{Re}\Sigma_+(\mathbf{0}, 0)$ and $\text{Im}\Sigma_+(\mathbf{0}, 0)$ vanish independently of T . The fact that $\Sigma^R(\mathbf{0}, 0)$ vanishes means the existence of a pole of the quark propagator at the origin; see eq. (2.9). The reason why $\text{Im}\Sigma_+(\mathbf{0}, 0)$ vanishes was explained before. The vanishing of the real part can be easily understood by the dispersion relation and the fact that $\text{Im}\Sigma_+(\mathbf{0}, \omega)$ is an even function of ω . Then we find that $\text{Re}\Sigma_+(\mathbf{0}, \omega)$ is an odd function of ω .

In Fig. 5, we show $|\text{Im}\Sigma_+(\mathbf{p}, \omega)|/g^2$ at finite momenta and energies at $T/m = 1.5$. The two separated peaks at $\mathbf{p} = \mathbf{0}$, coming from the Landau damping, tend to overlap with each other and are smeared as \mathbf{p} becomes large.

3.1.3. Asymptotic behavior in high temperature and weak coupling limit

Finally, let us consider the asymptotic behavior of $\Sigma^R(\mathbf{p}, \omega)$ in the high T and weak coupling limit, i.e., $gT \rightarrow \infty$ and $T/m \rightarrow \infty$ while $g^2T \rightarrow 0$.

In this limit, the leading contribution to the imaginary part $\text{Im}\Sigma^R(\mathbf{p}, \omega)$ comes from the terms which explicitly include the factor T^2 in eq. (3.10). Thus, the asymp-

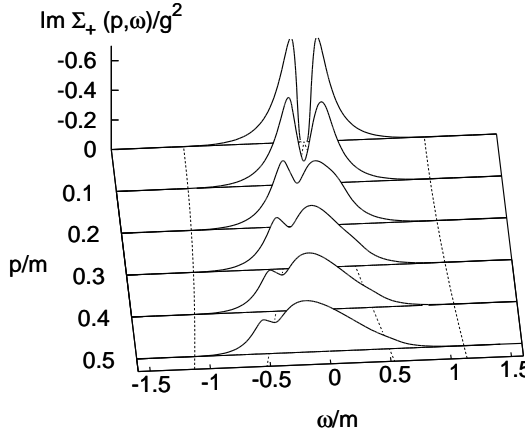


Fig. 5. The imaginary part of the self-energy $|\text{Im}\Sigma_+(\mathbf{p}, \omega)|$ for $T/m = 1.5$. The dashed lines in the $\omega\text{-}\mathbf{p}$ plane denote $\omega = \pm\sqrt{|\mathbf{p}|^2 + m^2}$ and $\omega = \pm\mathbf{p}$.

totic form of $\text{Im}\Sigma^R(\mathbf{p}, \omega)$ is given by

$$\text{Im}\Sigma^R(\mathbf{p}, \omega)|_{T \rightarrow \infty} = -\frac{\pi g^2 T^2}{32} \left(\frac{\gamma^0}{|\mathbf{p}|} - \frac{\omega \hat{\mathbf{p}} \cdot \boldsymbol{\gamma}}{\mathbf{p}^2} \right) \theta(\mathbf{p}^2 - \omega^2). \quad (3.13)$$

The real part in this limit is easily calculated using eq. (3.13) and the dispersion relation eq. (3.5). One then arrives at the following asymptotic form of $\Sigma^R(\mathbf{p}, \omega)$:

$$\Sigma^R(\mathbf{p}, \omega)|_{T \rightarrow \infty} = m_T^2 \frac{\gamma^0}{|\mathbf{p}|} Q(\mathbf{p}, \omega) + m_T^2 \frac{\hat{\mathbf{p}} \cdot \boldsymbol{\gamma}}{|\mathbf{p}|} \left(1 - \frac{\omega}{|\mathbf{p}|} Q(\mathbf{p}, \omega) \right), \quad (3.14)$$

with a thermal mass $m_T = gT/4$ and

$$Q(\mathbf{p}, \omega) = \frac{1}{2} \ln \left| \frac{\omega + |\mathbf{p}|}{\omega - |\mathbf{p}|} \right| - i \frac{\pi}{2} \theta(\mathbf{p}^2 - \omega^2). \quad (3.15)$$

Equation (3.14) is the same as the fermion self-energy of QED and QCD in the HTL approximation¹⁰⁾ apart from the definition of the thermal mass. Therefore, the quark spectrum in the Yukawa model in the limit $gT \rightarrow \infty$ ($T/m \rightarrow \infty$) and $g \rightarrow 0$ is equivalent to the well-known spectrum in the gauge theories.¹²⁾

We note that the analytic structure of the self-energy is changed qualitatively from that at intermediate T , i.e., at $T \simeq m$; there is no pole of the propagator at the origin any more in this limit, because $\text{Re}\Sigma_+(\mathbf{0}, \omega \rightarrow 0)$ behaves like $\sim 1/\omega$ and hence never vanishes, while $\text{Im}\Sigma_+(\mathbf{0}, \omega \rightarrow 0)$ vanishes. This change in the self-energy will reflect in that of the peak structure of the spectral function as discussed in the next subsection.

3.2. Quark spectral function at various temperatures

In this subsection, we examine how the quasi-particle picture of the quark changes at finite T using the quark spectral function $\rho_{\pm}(\mathbf{p}, \omega)$ and the quasi-dispersion

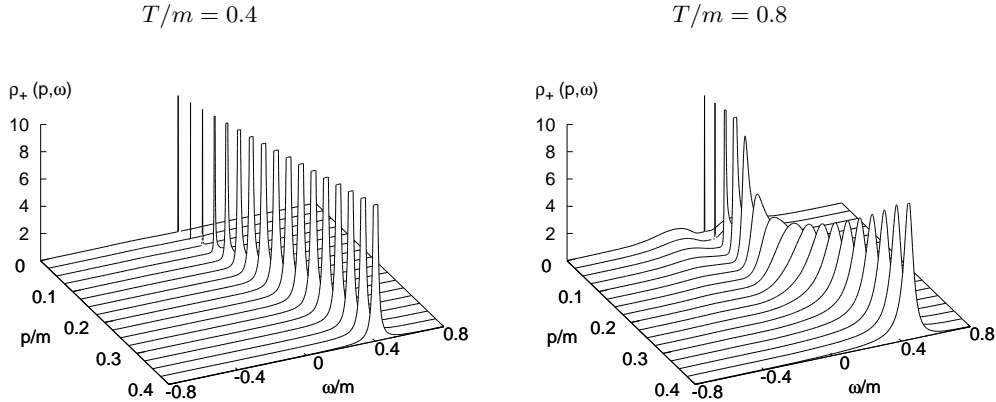


Fig. 6. The quark spectral function $\rho_+(\mathbf{p}, \omega)$ for $T/m = 0.4$ and $T/m = 0.8$.

relation $\omega_{\pm}(\mathbf{p})$. We fix the coupling constant as $g = 1$ through this subsection to see the T dependence of the spectrum. The g dependence will be discussed later. Since the dimensionful parameter in eq. (3.1) is only the boson mass m , we scale all the dimensionful parameters T, ω and \mathbf{p} by m .

3.2.1. Quark spectral function at zero temperature and the hard thermal loop approximation

Before showing the numerical results, we briefly review the quark spectrum at $T = 0$ and high T limit in our model. The analytic form of the quark self-energy at $T = 0$ is given in eq. (3.4). In this case the poles of the quark propagator are on the light cone $\omega = \pm|\mathbf{p}|$, since we have employed the on-shell renormalization condition to derive the self-energy eq. (3.4). The quark spectral functions $\rho_{\pm}(\mathbf{p}, \omega)$ are then given by

$$\rho_{\pm}(\mathbf{p}, \omega) = Z(0) \cdot \delta(\omega \mp |\mathbf{p}|) + \rho_{\pm}^{(\text{cont.})}(\mathbf{p}, \omega), \quad (3.16)$$

where the T -dependent residue $Z(T)$ is exactly unity at $T = 0$ under the on-shell renormalization condition and the continuum part $\rho_{\pm}^{(\text{cont.})}$ takes finite values for $|\omega| > \sqrt{\mathbf{p}^2 + m^2}$ *).

In the high T and weak coupling limit, the quark spectrum approaches the one calculated in the HTL approximation in the gauge theories with the thermal mass $m_T = gT/4$ as the quark self-energy does; see the previous subsection. In this limit, both $\rho_{\pm}(\mathbf{p}, \omega)$ have two delta-functions corresponding to the normal quasi-particle and plasmino excitations in addition to the continuum part in the space-like region,^{10),14)} see eqs.(3.14) and (3.15). In the high T limit with fixed g , these two peaks have the width of the order gm_T .¹⁰⁾

*⁾ Some readers may worry about the violation of a sum rule for the spectral function, $\int_{-\infty}^{\infty} d\omega \rho_{\pm}(\mathbf{p}, \omega) = 1$. In the relativistic field theory, this sum rule does not necessarily hold when the renormalization has been made.¹⁰⁾

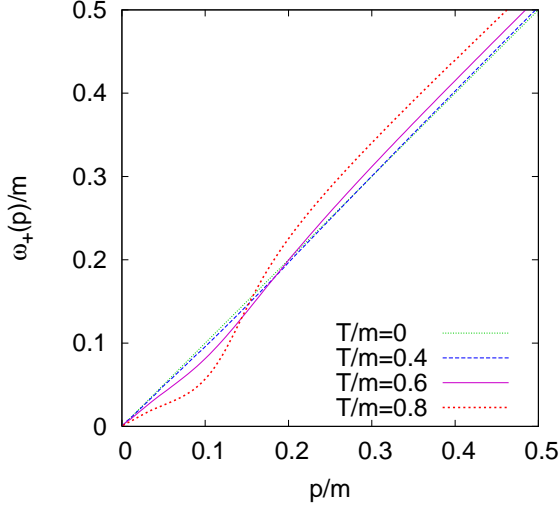


Fig. 7. The quasi-dispersion relation $\omega_+(\mathbf{p})$ for several values of T .

3.2.2. Quark spectral function at low temperature

In Figs. 6 and 7, we show the spectral function $\rho_+(\mathbf{p}, \omega)$ and the quasi-dispersion relation $\omega_+(\mathbf{p})$ of the quark part for relatively low temperatures, i.e., $T < m$. The anti-quark parts ρ_- and $\omega_-(\mathbf{p})$ can be figured out by the symmetric properties eq. (2.8) and $\omega_-(\mathbf{p}) = -\omega_+(\mathbf{p})$. At $T/m = 0.4$, the spectral function $\rho_+(\mathbf{p}, \omega)$ and $\omega_+(\mathbf{p})$ are almost the same as that at $T = 0$; $\rho_+(\mathbf{p}, \omega)$ has sharp quasi-particle peaks around $\omega = |\mathbf{p}|$, and $\omega_+(\mathbf{p}) \simeq |\mathbf{p}|$. At $T/m = 0.8$, the quasi-particle peaks are clearly bended around $|\mathbf{p}|/m = 0.15$. The quasi-dispersion relation also deviates from the free one around $|\mathbf{p}|/m = 0.15$. We notice that it shows an unphysical acausal behavior; the imaginary part of the self-energy is large in this momentum region as shown in Fig. 8, and thus the quasi-dispersion relation becomes unphysical in this region.

To understand the behavior of $\rho_+(\mathbf{p}, \omega)$ and $\omega_+(\mathbf{p})$ in Figs. 6 and 7, we show the real and imaginary parts of $\Sigma_+(\mathbf{p}, \omega)$ at $T/m = 0.8$ and several momenta in the left panel of Fig. 8. We see that there are two peaks in $\text{Im}\Sigma_+(\mathbf{0}, \omega)$ in positive- and negative-energies corresponding to the terms (II) and (III) in eq. (3.6), respectively. One sees that $\text{Re}\Sigma_+(\mathbf{p}, \omega)$ shows a steep rise in the two regions corresponding to these peaks. We also show the lines $\omega - |\mathbf{p}|$, i.e., l.h.s. of eq. (2.10) by dotted lines in Fig. 8. Since the quasi-dispersion $\omega_+(\mathbf{p})$ is given by eq. (2.10), $\omega_+(\mathbf{p})$ is graphically given by the crossing points between the dotted lines and $\text{Re}\Sigma_+(\mathbf{p}, \omega)$. We see that the crossing points strongly depend on the shape of $\text{Re}\Sigma_+(\mathbf{p}, \omega)$. Around $\omega/m = 0.1$, the bending of $\text{Re}\Sigma_+(\mathbf{p}, \omega)$ makes the quasi-dispersion relation deviate from the free quark dispersion, as shown in Fig. 7.

3.2.3. Quark spectral function at intermediate temperature

As T is raised further so that T becomes comparable with m , $\rho_\pm(\mathbf{p}, \omega)$ and $\omega_\pm(\mathbf{p})$ make a drastic change; notice that the bosons get to be thermally excited with a

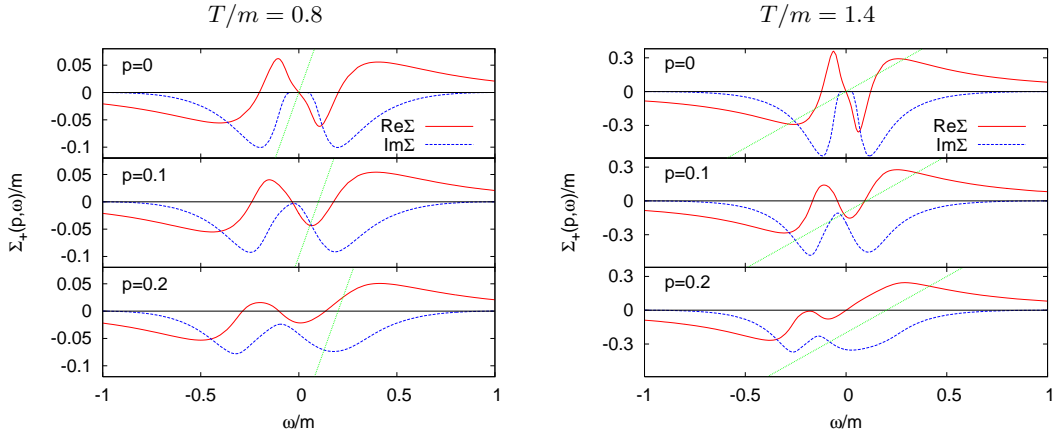


Fig. 8. The quark self-energy $\Sigma_+(\mathbf{p}, \omega)$ for several momenta at $T/m = 0.8$ and 1.4 . The dotted straight line denotes the l.h.s. in eq. (2.10), i.e., $\omega - |\mathbf{p}|$.

considerable probability at such a temperature. In the left panels of Fig. 9, we show $\rho_+(\mathbf{p}, \omega)$ at $T/m = 1.0, 1.4$ and 1.8 . We see that at $T/m = 1.0$, the quasi-particle peak starts to split around $|\mathbf{p}|/m = 0.15$. At the same time, there appear broad peaks both in the positive- and negative-energy regions for lower momenta: Thus the spectral function in the low-momentum region has *three peaks*.

A remark is in order here: Among the three peaks, the one around the origin is of the delta function and thus it is difficult to read off the strength from Fig. 9. Here we notice that the strength at the origin is actually given by the residue of the Green functions, G_{\pm} : The residue is simply given by

$$Z(T) = [1 - \partial \text{Re} \Sigma_{\pm} / \partial \omega]^{-1}, \quad (3.17)$$

since the imaginary part $\text{Im} \Sigma_{\pm}(\mathbf{p}, \omega)$ vanish at the origin. The T -dependence of $Z(T)$ is shown in Fig. 10; $Z(0) = 1$ as mentioned before, and $Z(T)$ decreases gradually as T is raised but still takes considerable values at $T/m \sim 1$, and hence the three-peak structure of the spectral function is realized in this temperature region as mentioned before.

In the high T limit, $Z(T)$ vanishes and only two peaks remain in $\rho_{\pm}(\mathbf{p}, \omega)$: As we will see later, these two peaks correspond to the normal quark quasi-particle and plasmino excitations obtained in the HTL approximation.

In the right panels of Fig. 9, we show the quasi-dispersion relations and the (ω, p) -dependence of the spectral function; the latter of which is represented by the (color) density. In these panels, ω_+ (ω_-) and ρ_+ (ρ_-) are shown in the right (left) half of the figures. Note that the direction of the momentum scale in the left half plane is opposite to that of the right half plane. At $T/m = 1$, there is one quasi-dispersion curve for the whole momentum region. As T becomes larger, the quasi-dispersion curve greatly bends to make ‘back-bending’ parts, and there eventually appear multi-valued quasi-dispersion relations for some momentum region. At $T/m = 1.4$, the quasi-dispersion relation is five-valued at low momenta; notice that the back-bending quasi-dispersion relation is acausal and unphysical. Only the three of them, however,

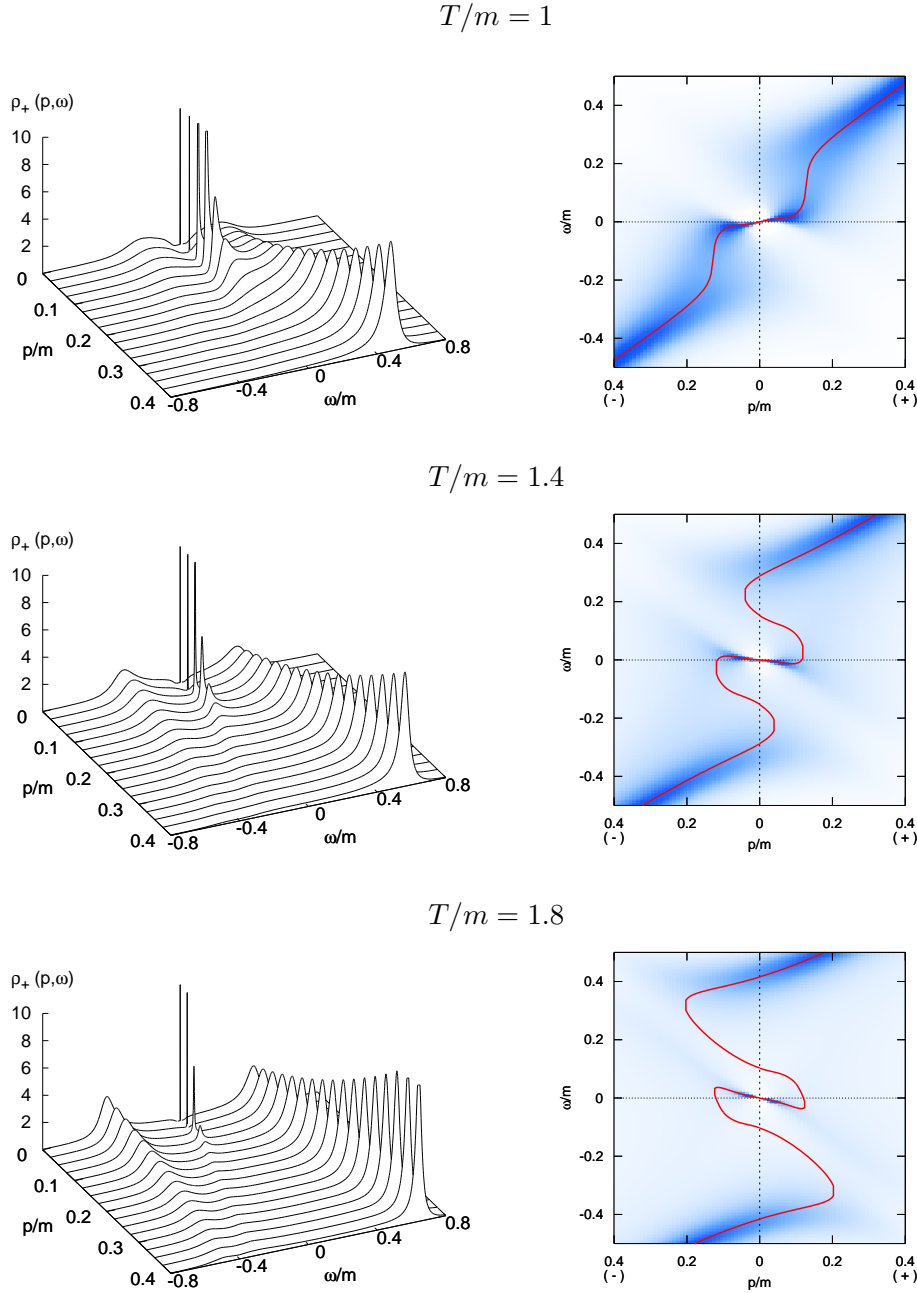


Fig. 9. The quark spectral function $\rho_+(\mathbf{p}, \omega)$ (left) and the quasi-dispersion relations $\omega_{\pm}(\mathbf{p})$ (right) for $T/m = 1.0, 1.4$, and 1.8 from the top. In the right panels, (ω, \mathbf{p}) -dependence of $\rho_{\pm}(\mathbf{p}, \omega)$ is represented by the color density. $\omega_+(\omega_-)$ and $\rho_+(\rho_-)$ are shown in the right (left) half in these panels; notice the direction of the momentum scale in the left half plane is opposite to that of the right half plane.

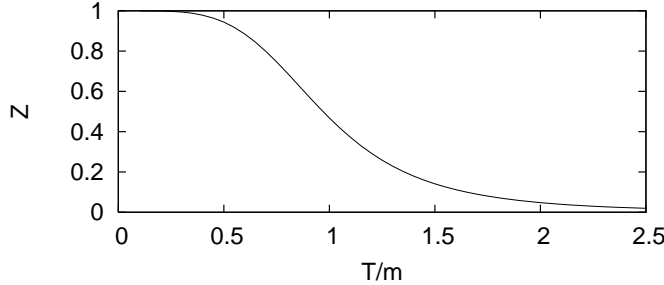


Fig. 10. The temperature dependence of the residue of the pole at the origin ($\omega = |\mathbf{p}| = 0$).

are accompanied with the peaks of the spectral function, while the other two are not: The quasi-dispersion relation $\omega_+(\mathbf{p})$ around the back-bending region does not form a peak in $\rho_+(\mathbf{p}, \omega)$ and unphysical. The back-bending feature of the quasi-dispersion relation becomes more prominent as T is raised further, as shown in the bottom-right panel in Fig. 9.

To understand the peculiar behavior of $\rho_+(\mathbf{p}, \omega)$ and $\omega_+(\mathbf{p})$ in Fig. 9, we show $\Sigma_+(\mathbf{p}, \omega)$ at an intermediate temperature $T/m = 1.4$ in the right panel of Fig. 8. We see that the two peaks in $\text{Im}\Sigma_+(\mathbf{p}, \omega)$ become sharper than those for $T/m = 0.8$ shown in the left panel and the oscillatory change of the real part around $\omega \sim 0$ also becomes more prominent. In order to find out the quasi-dispersion relation $\omega_+(\mathbf{p})$, i.e., the solutions of eq. (2.10), from the figure, we draw the line $\omega - |\mathbf{p}|$, i.e., l.h.s. of eq. (2.10). In the top panel, we see that there appear five crossing points. The crossing points with the second and fourth largest ω , however, are located at the energies of the peak of $|\text{Im}\Sigma_+(\mathbf{p}, \omega)|$ and hence the spectral function does not form a peak there. For large momenta, the number of the crossing points decreases and eventually only one crossing point remains.

3.2.4. Quark spectral function at high temperature

Here we examine the quark spectrum at higher temperatures. We show $\rho_+(\mathbf{p}, \omega)$ and $\omega_\pm(\mathbf{p})$ at $T/m = 2.5$ in Fig. 11, as an example of the high-temperature case, i.e., $T \gg m$. One sees that two well-formed peaks are seen in the positive- and negative-energy regions, while the peak around the origin is immediately disappears as the momentum becomes finite. On the other hand, one sees a complicated curve of the quasi-dispersion relation in the right panel: It should be noted that the back-bending behavior of the quasi-dispersion relation, however, is not physical, nor corresponds to a peak of the spectral function as mentioned before. We show the quasi-dispersion relation at some temperatures, $T/m = 2, 3$ and 5 , in the high- T region, in Fig. 12 together with that in the HTL approximation with the thermal mass $m_T = gT/4$. From the figures, it is nicely seen that our quasi-dispersion relation approaches that obtained in the HTL approximation as T is raised; the two of $\omega_+(\mathbf{k})$ approaches the quark quasi-particle and plasmino dispersion relations, respectively, having the

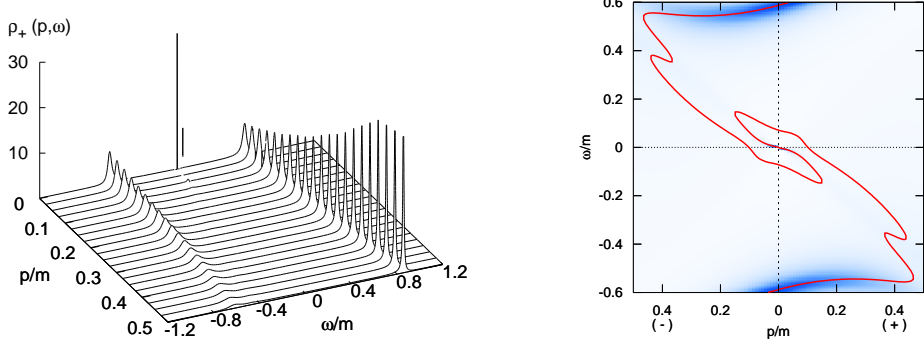


Fig. 11. The quark spectral function $\rho_+(\mathbf{p}, \omega)$ and the quasi-dispersion relation $\omega_{\pm}(\mathbf{p})$ at $T/m = 2.5$.

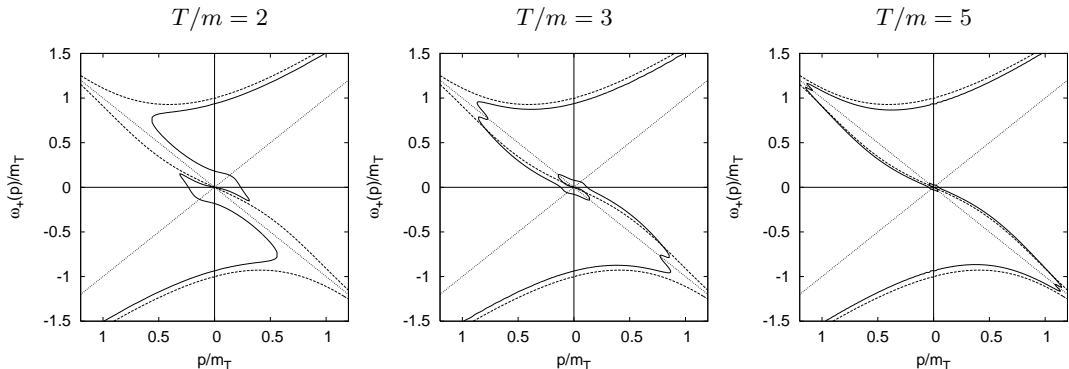


Fig. 12. The quasi-dispersion relations $\omega_{\pm}(\mathbf{p})$ at $T/m = 2, 3$ and 5 . All the values are in the unit of the thermal mass $m_T = gT/4$. The dashed line denotes the dispersion relation in the HTL approximation.

thermal mass $m_T = gT/4$ *).

Here we notice that there appears a continuous spectral bump at $\omega \sim 0$ in the space-like region in the HTL approximation, which is reminiscent of the spectral peak seen at intermediate temperatures in the space-like region around $\omega = 0$. It should be stressed that the physical origin of the peak is, however, completely different from each other; the peak seen in the intermediate temperatures is due to the pole of the Green function as shown in the previous subsection, while the bump in the HTL approximation is owing to the Landau damping, and the quark propagator calculated in this approximation does not have a pole at $\omega = 0$.

^{*)} In fact, the spectrum in Fig. 12 does not exactly coincide with that in the HTL approximation because the coupling is not small. However, it is known that the difference is small at the one-loop order.²³⁾

3.3. Discussion on three-peak structure of spectral function at $T \sim m$

Now we have seen that the appearance of the three-peak structure at T comparable with the boson mass m is the most characteristic feature in the quark spectral function caused by the coupling with the massive boson. In this subsection, we try to elucidate the physical origin of the multi-peak structure. The discussion will proceed as the one⁷⁾ given for the origin of the three-peak structure caused by the soft mode of the chiral phase transition.

To understand the physical mechanism for realizing the three-peak structure of $\rho_+(\mathbf{p}, \omega)$, we first recall that there develop two peaks in $\text{Im}\Sigma_+$ at a positive and negative energy in this temperature region; the peak height there grows as T is raised. As was discussed in Section 3.1, these two peaks correspond to the decay processes depicted by (II) and (III) in Fig. 3, which are both Landau damping: The process (II) is the annihilation process of the incoming quark Q and the thermally excited antiquark into a boson in the thermal bath, $Q + \bar{q} \rightarrow b$, and its inverse process. Two remarks are in order here: (1) The disappearance of an anti-quark means a creation of a 'hole' in the thermally excited anti-quark distribution.¹⁴⁾ (2) The creation of a boson in a thermal bath at a temperature is enhanced in comparison with the case in the vacuum by a statistical factor $1 + n$, which becomes large when T is as high as about the value of m . Thus one sees that the process (II) causes a virtual mixing between the quark and 'anti-quark hole' states by the coupling with the boson in a thermal bath *), which mixing gets enhanced when $T/m \sim 1$.

The process (III) is another decay process of a quasi-quark state Q , which is now understood to be a mixed state of quarks and antiquark-holes, into an on-shell quark via a collision with the thermally excited boson; $Q + b \rightarrow q$ and its inverse process, $q \rightarrow Q + b$. As is seen from the left panel of Fig.2, the involved energy for probable processes which occur at small momenta is negative for the process (III). These processes again give rise to a mixing of a quasi-quark and an anti-quark hole state. As seen by the Bose-Einstein distribution function n , the thermally excited bosons are abundant when T becomes a large value as m .

A similar interpretation holds for the anti-quark sector, $\text{Im}\Sigma_-(\mathbf{p}, \omega)$, if the quark and the anti-quark hole are replaced by an anti-quark and a quark hole, respectively. Thus, the process corresponding to (II) in Fig.3 is $\bar{Q} + q \rightarrow b$, where q denotes a thermally excited quark, for instance. So we shall from now on discuss only the quark sector.

The mixing mechanism of the quark and the hole state can be also characterized as a *resonant scattering*,²⁰⁾ which is originally introduced to understand the non-Fermi liquid behavior of the fermion near but above the critical temperature of the superconducting transition.^{19), 20)} In fact, we have seen that the process (II) in Fig.3 includes a scattering process of the quark by the massive boson to create a hole state in the thermally distributed anti-quark states; $Q \rightarrow \bar{q}_h + b$. Such a process is called the resonant scattering.²⁰⁾ Notice that the most probable process at finite T involves the lowest energy state of the boson, i.e., the rest boson with the energy m .

*) We remark that the quark number conservation is not violated with this mixing, since the 'anti-quark hole' has a positive quark number.

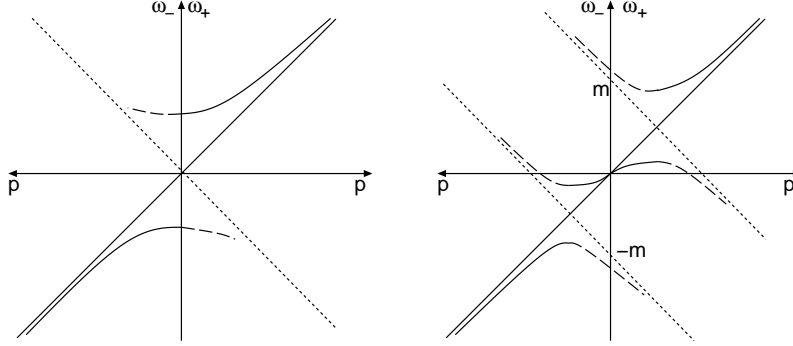


Fig. 13. Typical peak position of the spectral functions in case of the level mixing at the origin (left) and away from the origin (right). The long dashed line denotes that the strength of the spectrum is getting weaker. The solid straight line denotes the free quark and antiquark dispersion relations, and the dotted line the antiquark hole and quark hole ones. The level repulsion takes place at the crossing point of the two types of the straight lines.

The energy conservation laws in the most probable case for the above process reads $\omega_Q(\mathbf{p}) + \omega_{\bar{q}}(-\mathbf{p}) = m$ or equivalently,

$$\omega_Q(\mathbf{p}) = m - \omega_{\bar{q}}(-\mathbf{p}). \quad (3.18)$$

This equation actually represents the energy-momentum relation for the particles involved in the state mixing; thus one sees that the physical energy spectrum is obtained as a result of the level repulsion between the energies $\omega_q(\mathbf{p}) = |\mathbf{p}|$ and $m - \omega_{\bar{q}}(-\mathbf{p}) = m - |\mathbf{p}|$ in the perturbative picture. This situation is shown in the upper-right part in the right panel of Fig.13.

Similarly, the process (III) in Fig.3 includes the process $q \rightarrow Q + b$, and the energy-momentum conservation law for this process reads for the most probable case

$$-\omega_q(\mathbf{p}) = -m + \omega_Q(\mathbf{p}). \quad (3.19)$$

Thus, the physical energy spectrum is obtained as a result of the level repulsion between the energies $-|\mathbf{p}|$ and $-m + |\mathbf{p}|$. This situation is also shown in the lower-right part in the right panel of Fig.13.

Thus at temperatures $T/m \sim 1$ owing to the finite boson mass, the level repulsions occur far from the origin and then the quasi-dispersion relations are bended twice, or the two gap-like structures in the quark spectrum are formed at the positive- and negative-energies, as shown in the right panel of Fig. 13.

It is interesting to consider the high temperature limit $T \gg m$, or $m/T \sim 0$, for which the effect of the boson mass can be neglected and the resonant scattering occurs only once at the origin ($\omega = |\mathbf{p}| = 0$) since the energy levels which are to be repelled cross only there. Then the situation becomes what is represented in the left panel of Fig. 13.

It has been shown⁷⁾ that the quark spectral function shows a three-peak structure near T_c of the chiral transition when the chiral soft mode⁴⁾ is incorporated

in the quark self-energy. As was described in Introduction, the soft modes behave as if a massive elementary boson with a mass $m_\sigma^*(T)$ as T approaches T_c , $\omega_{\text{soft}} \sim \sqrt{\mathbf{p}^2 + m_\sigma^*(T)^2}$ and hence the quark spectra discussed in 7) is essentially the same as that treated in this section. We also notice that as T is lowered toward T_c , $m_\sigma^*(T)$ tends to vanish and hence the ratio $T/m_\sigma^*(T)$ becomes large so the quark spectrum approaches that in the $T/m \rightarrow \infty$ limit of the present work, as is the case.⁷⁾

3.4. Quark spectral function at various coupling constants

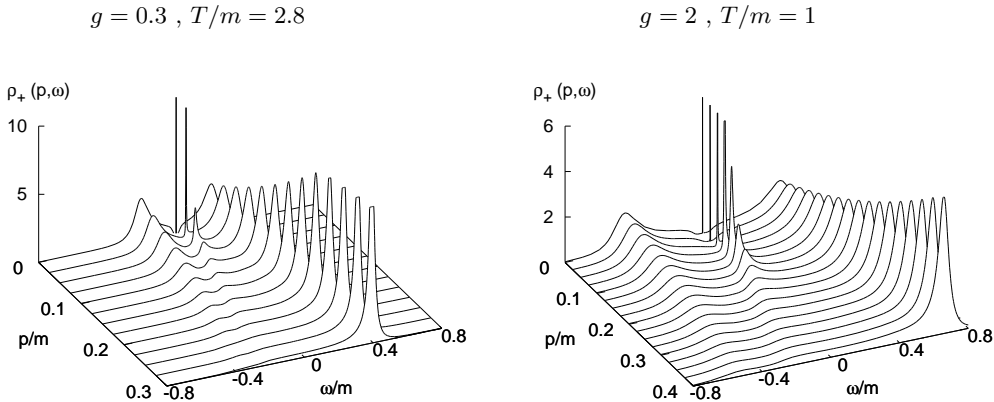


Fig. 14. The quark spectral functions $\rho_+(\mathbf{p}, \omega)$ at $g = 0.3$, $T/m = 2.8$ and $g = 2$, $T/m = 1$.

We have seen the quark spectrum with a fixed coupling $g = 1$, where we have found the novel three-peak structure at intermediate temperatures. How do these features change with a variation of g ? In the previous subsections, we have pointed out that the Landau damping, which induces the two peaks in $\text{Im}\Sigma^R(\mathbf{p}, \omega)$, plays an essential role to give rise to the three-peak structure in the quark spectrum. Since $\Sigma^R(\mathbf{p}, \omega)/g^2$ is independent of g in the one-loop order, we can expect that the three-peak structure in the quark spectrum is not affected qualitatively even if we vary the coupling g . We checked numerically that this is indeed the case: There appears similar three-peak structure in the quark spectrum irrespective of g , although the temperature at which the clear three-peak structure appears depends on g .

In Fig. 14, we show the quark spectral function $\rho_+(\mathbf{p}, \omega)$ for $g = 0.3$ and 2 , at T where a clear three-peak structure is seen. The spectral function shows a single-peak structure at T lower than that shown in Fig. 14, and approaches the two-peak structure at higher T . It is notable that for larger g , the three-peak structure appears at lower T and the distance between the peaks becomes larger.

§4. Quark spectrum in Yukawa model with massive vector (axial-vector) boson

In this section, we investigate the quark spectrum using a Yukawa model with a massive vector (axial-vector) boson and show that the three-peak structure of the quark spectral function is obtained.

We start from the following Lagrangian composed of a massless quark ψ and vector boson field V_μ ;

$$\mathcal{L} = \bar{\psi}(i\partial - ig\gamma^\mu V_\mu)\psi + \mathcal{L}_v. \quad (4.1)$$

As for the Lagrangian of the massive vector field \mathcal{L}_v , we consider the following simplest form;

$$\mathcal{L}_v = -\frac{1}{4}F_{\mu\nu}F^{\mu\nu} + \frac{1}{2}m^2V_\mu V^\mu, \quad (4.2)$$

with the field strength $F_{\mu\nu} = \partial_\mu V_\nu - \partial_\nu V_\mu$.

As is the case for the scalar boson, we shall see that the replacement of the vector boson with an axial-vector one does not lead to any difference in the quark spectrum in the perturbation theory, which is taken in this work.

4.1. Quark self-energy

In the one-loop order, the quark self-energy in the imaginary time formalism is given by

$$\tilde{\Sigma}(\mathbf{p}, i\omega_m) = -g^2 T \sum_n \int \frac{d^3\mathbf{k}}{(2\pi)^3} \gamma^\mu \mathcal{G}_0(\mathbf{k}, i\omega_n) \gamma^\nu \mathcal{D}_{\mu\nu}(\mathbf{p} - \mathbf{k}, i\omega_m - i\omega_n), \quad (4.3)$$

with the Matsubara propagator for the massive vector boson

$$\mathcal{D}_{\mu\nu}(i\nu_n, \mathbf{p}) = -\frac{g_{\mu\nu} - \tilde{p}_\mu \tilde{p}_\nu / m^2}{\tilde{p}_\mu \tilde{p}^\mu - m^2}, \quad (4.4)$$

where $\tilde{p}_\mu = (i\nu_n, \mathbf{p})$. The propagator for the vector boson eq. (4.4), which is obtained from eq. (4.2), is called the Proca propagator.²⁴⁾ It is known that one can not take the massless limit of eq. (4.4), because of the lack of gauge invariance in eq. (4.2). As we will see later, this property causes a difficulty in the the high temperature limit $T/m \rightarrow \infty$ because this limit also represents the massless limit with fixed T . One should describe a boson field in the Stuckelberg formalism²⁴⁾ which has the massless limit, if we study the spectrum at high T . In this work, since we explore the qualitative effect of the phenomenological massive vector boson on the quark spectrum at intermediate T , we do not consider this difficulty associated with the Proca propagator.

For the coupling with an axial-vector boson, the self-energy is the same form as eq. (4.3), because the γ_5 matrices in the vertices are canceled out for the massless quark propagator \mathcal{G}_0 . Therefore, the following results hold also for the coupling with an axial-vector boson, as is mentioned above.

Taking the summation of the Matsubara mode and the analytic continuation $i\omega_n \rightarrow \omega + i\eta$ for eq. (4.3) (see Appendix B for the detail.), we obtain

$$\Sigma^R(\mathbf{p}, \omega) = g^2 \sum_{s,t=\pm} t \int \frac{d^3\mathbf{k}}{(2\pi)^3} \frac{\gamma^\mu \Lambda_s(\mathbf{k}) \gamma^0 \gamma^\nu}{2E_b} \left(g_{\mu\nu} - \frac{q_\mu q_\nu}{m^2} \right) \frac{f(sE_f) + n(-tE_b)}{\omega + i\eta - sE_f - tE_b}, \quad (4.5)$$

with $q_\mu = (\omega - E_f, \mathbf{p} - \mathbf{k})$. In order to eliminate the ultraviolet divergence in eq. (4.5), we employ the same strategy as in the previous section: We first divide eq. (4.5) into T -independent and T -dependent parts as $\Sigma^R(\mathbf{p}, \omega) = \Sigma^R(\mathbf{p}, \omega)_{T=0} + \Sigma^R(\mathbf{p}, \omega)_{T \neq 0}$ and calculate $\Sigma^R(\mathbf{p}, \omega)_{T=0}$ imposing the renormalization condition.

In the present case, however, unlike the previous section the T -independent part $\Sigma^R(\mathbf{p}, \omega)_{T=0}$ includes a divergence in the term proportional to \not{p}^3 and the on-shell renormalization condition can not solely eliminate the divergence (See, Appendix C). This is due to the bad ultraviolet behavior coming from the Proca propagator $D_{\mu\nu}^R$ in the real-time. Here we impose an renormalization condition $\partial^3 \Sigma^R(p)/\partial \not{p}^3|_{\not{p}=0} = 0$ to eliminate this divergence and obtain the following renormalized form,

$$\begin{aligned} \Sigma^R(p)_{T=0} = & \frac{g^2}{32\pi^2} \not{p} \left(\frac{P^2 + 2m^2}{m^2} \frac{(P^2 - m^2)^2}{P^4} \log \left| \frac{m^2 - P^2}{m^2} \right| - \frac{5}{6} \frac{P^2}{m^2} - 2 + 2 \frac{m^2}{P^2} \right) \\ & - i \frac{g^2}{32\pi^2} \not{p} \frac{P^2 + 2m^2}{m^2} \frac{(P^2 - m^2)^2}{P^4} \epsilon(p_0) \theta(P^2 - m^2). \end{aligned} \quad (4.6)$$

The T -dependent part $\Sigma^R(\mathbf{p}, \omega)_{T \neq 0}$ can be calculated by the same procedure as in the previous section; i.e., we first calculate the imaginary part $\text{Im}\Sigma^R(\mathbf{p}, \omega)_{T \neq 0}$ and then derive the real part using the dispersion relation eq. (3.5).

From eq. (4.5), we obtain

$$\begin{aligned} \text{Im}\Sigma^R(\mathbf{p}, \omega) = & -\pi g^2 \int \frac{d^3\mathbf{k}}{(2\pi)^3} \frac{\gamma^\mu \Lambda_s(\mathbf{k}) \gamma^0 \gamma^\nu}{2E_b} \left(g_{\mu\nu} - \frac{q_\mu q_\nu}{m^2} \right) \\ & \times \{ -(1+n-f)\delta(\omega - E_f - E_b) - (n+f)\delta(\omega + E_f - E_b) \\ & + (n+f)\delta(\omega - E_f + E_b) + (1+n-f)\delta(\omega + E_f + E_b) \}. \end{aligned} \quad (4.7)$$

with $n = n(E_b)$ and $f = f(E_f)$. The four terms in eq. (4.7) have the same statistical factors and the delta functions as those in eq. (3.6), which means that the decay processes of the quasi-particles described by these terms can be understood diagrammatically as shown in Fig.3. The region in the energy-momentum plane where each term has a finite value is the same as Fig. 2.

For zero momentum $\mathbf{p} = \mathbf{0}$, we obtain

$$\text{Im}\Sigma_\pm(\mathbf{p} = \mathbf{0}, \omega) = -\frac{g^2}{32\pi} \frac{\omega^2 + 2m^2}{m^2} \frac{(\omega^2 - m^2)^2}{\omega^3} \left(\coth \frac{\omega^2 + m^2}{4T\omega} + \tanh \frac{\omega^2 - m^2}{4T\omega} \right). \quad (4.8)$$

Equation (4.8) differs from eq. (3.11) in the Yukawa model with the scalar boson by a factor $(\omega^2 + 2m^2)/m^2$. For small energy $\omega \lesssim m$, this term approximately gives an

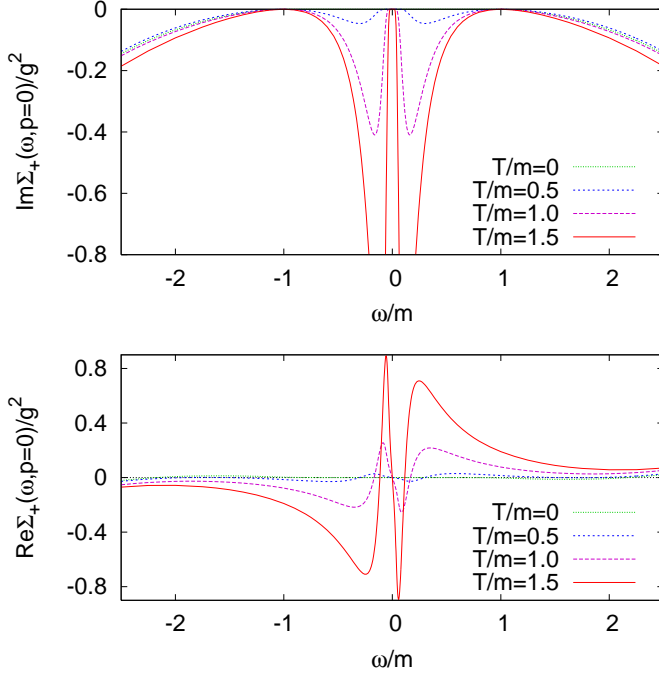


Fig. 15. The imaginary and real parts of the self-energy $\Sigma_+(\mathbf{p}, \omega)$ at zero momentum for several temperatures.

overall factor 2. Therefore, we expect that the two-peak structure of $\text{Im}\Sigma_{\pm}(\mathbf{p} = 0, \omega)$ caused by the Landau damping at $|\omega| < m$ and hence the three-peak structure in the quark spectral function do not alter qualitatively even in the present case. For large ω , on the other hand, the factor behaves as ω^2/m^2 , which makes eq. (4.8) much larger than that of eq. (3.11) for $|\omega| \gg m$, leading to a difference between the scalar and the vector boson at very high T .

4.2. Quark spectrum at intermediate temperatures

In Fig. 15, we show the imaginary and real parts of $\Sigma_+(\mathbf{p}, \omega)$ for $\mathbf{p} = 0$ at $T/m = 0, 0.5, 1$ and 1.5 . We fix the coupling constant as $g = 1$. As can be deduced from the above discussions, the qualitative features of both parts for $|\omega|/m < 1$ are quite similar as that in Fig. 4: There are clear two peaks in $\text{Im}\Sigma_+$ at $|\omega|/m < 1$ and oscillating behavior in $\text{Re}\Sigma_+(\mathbf{p} = 0, \omega)$, and they grow rapidly as T increases. For $|\omega|/m > 1$, one sees that $|\text{Im}\Sigma_+(\mathbf{p} = 0, \omega)|$ grows more rapidly than that in the Yukawa model with the scalar boson shown in Fig. 4.

In Fig. 16, we show $|\text{Im}\Sigma_+(\mathbf{p}, \omega)|$ in the energy-momentum plane at $T/m = 1.5$. One sees that the qualitative feature of $|\text{Im}\Sigma_+(\mathbf{p}, \omega)|$ is again almost the same as that in Fig. 5 at the range $|\omega|/m \lesssim 1$.

In Fig. 17, we show the quark spectral function for $T/m = 0.4, 0.8, 1.0$ and 1.2 . One sees that there appears a three-peak structure at intermediate temperatures, as was seen in the previous section. This is quite natural and would be expected from the behavior of the self-energy. The clear three-peak structure is formed at lower

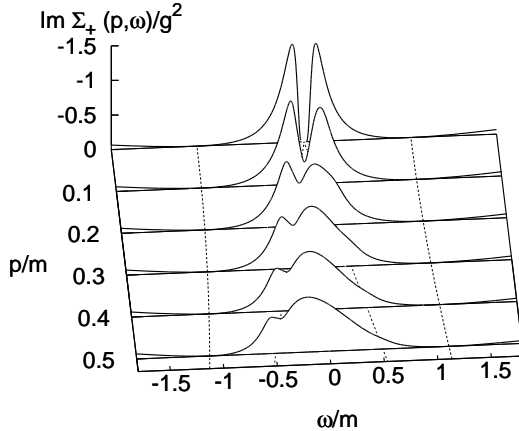


Fig. 16. The imaginary part of the self-energy $|\text{Im}\Sigma_+(\mathbf{p}, \omega)|$ at $T/m = 1.5$.

T than that in the scalar boson case. This is because the term $(\omega^2 + 2m^2)/m^2$ in eq. (4.8), which gives approximately a factor 2 at $\omega \lesssim m$, plays a role to enhance the coupling constant g . As discussed in Subsection 3.4, the temperature at which the clear three-peak structure appears decreases for larger g .

4.3. Quark spectrum at high temperatures

Next, we show the quark spectral function at higher temperatures $T/m = 5$ and 10 in Fig. 18. We find that the energy at the quasi-particle peak saturates around $\omega/m = 2.5$ at $\mathbf{p} = 0$. It is also noteworthy that the two peaks having the finite thermal mass become obscure as T is raised.

In order to understand this behavior of $\rho_+(\mathbf{p}, \omega)$ at higher T , in Fig. 19 we show the self-energy at $T/m = 0, 5, 10$, and 15 . In the right figure, we show a straight line $\text{Re}\Sigma_+ = \omega$ in order to see the quasi-dispersion relation. At $T = 0$, there exist three quasi-dispersion relations at $\omega = 0$ and around $\omega \simeq \pm 10m$. The latter two solutions are unphysical ones^{*)}. In Fig. 19, it is also noteworthy that the $\text{Re}\Sigma_+$ changes its sign around $\omega = 2.5m$ for higher T . In fact, we can analytically prove that the zero of $\text{Re}\Sigma_+$ approaches $\omega = \sqrt{6}m$ in the high T limit (see Appendix D). Due to this property, the solution of the quasi-dispersion relation corresponding to the two peaks in Fig. 17 approaches $|\omega| = \sqrt{6}m$ at $\mathbf{p} = 0$ in the high T limit.

§5. Summary and concluding remarks

We have investigated the quasi-particle picture of a fermion, which we called a “quark” in this paper, in Yukawa models composed of a massless quark and a

^{*)} These quasi-dispersion relations do not form a peak in the quark spectral function, because the $|\text{Im}\Sigma^R|$ takes a large value there. We have confirmed that they also exist for very large values of ω in the model with the scalar boson in Sec.3.

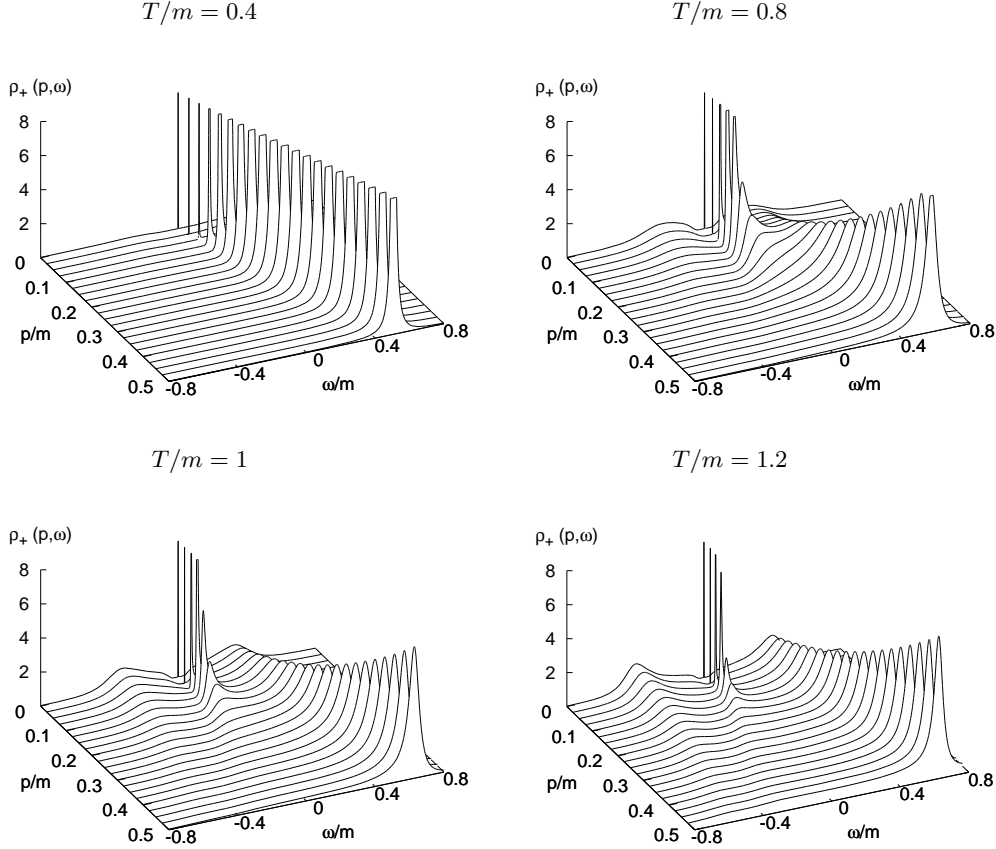


Fig. 17. The quark spectral function $\rho_+(\mathbf{p}, \omega)$ for $T/m = 0.4, 0.8, 1$ and 1.2 .

massive boson at finite temperature (T). We have considered four-types of massive bosons, i.e., scalar, pseudoscalar, vector and axial-vector bosons with a mass m , though the scalar (vector) and the pseudoscalar (axial-vector) bosons do not lead to any difference in the quark spectrum, since the quark is massless. The Proca formalism is employed for the vector boson. For both the models, the quark self-energy is computed up to the one-loop order and the spectral function and the quasi-dispersion relation of the quark are studied. We have found that the quark spectral function at low frequency and low momentum is strongly modified from the free quark spectrum, and has a three-peak structure at intermediate T , i.e., at $T/m \sim 1$. We have noticed that the number of the branches of the quasi-dispersion relation does not necessarily coincide with that of the peaks in the fermion spectral function, when the imaginary part of the quark self-energy is large. We have shown that the two of the three peaks have finite thermal masses and approach the normal quasi-quark and plasmino excitations in the HTL approximation in the high T limit, while the strength of the peak at the origin becomes weaker and disappears in this limit. In the Yukawa model with the vector boson, we have found that the behavior

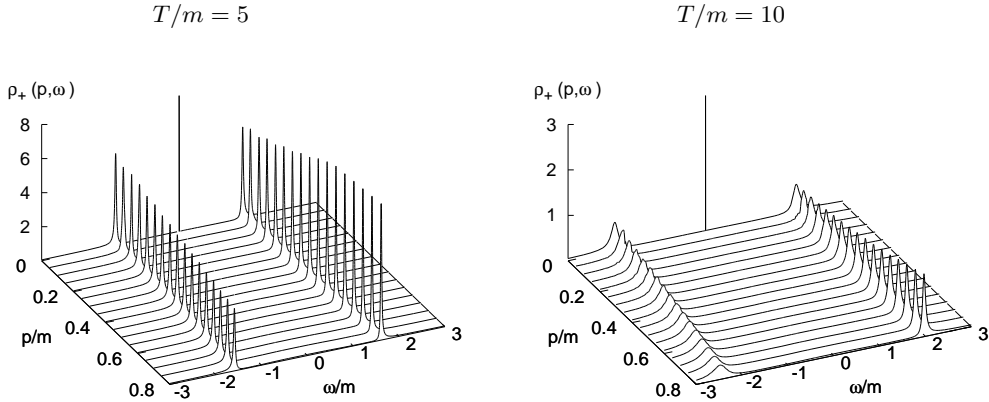


Fig. 18. The quark spectral function $\rho_+(\mathbf{p}, \omega)$ at $T/m = 5$ and 10 .

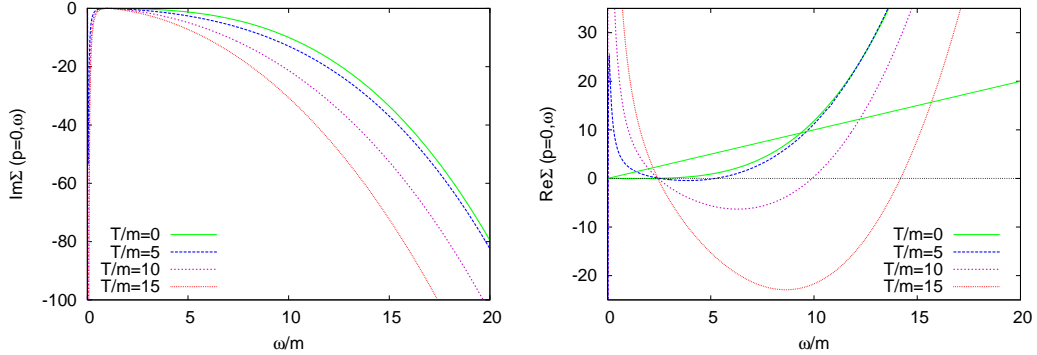


Fig. 19. The imaginary and real parts of the self-energy $\Sigma_+(\mathbf{p}, \omega)$ at zero momentum at $T/m = 5, 10$ and 15 .

of the spectral function is not altered from that in the Yukawa model with the scalar boson up to $T \approx m$. In the high T limit, the spectrum in the Proca formalism does not approach the one in the HTL approximation.

We have discussed that the three-peak structure originates from the Landau damping, that is, the scattering processes of a quark and an antiquark hole of a thermally excited antiquark, and of an antiquark and a quark hole of a thermally excited quark. They induce a formation of energy gaps in the quark spectrum owing to the level mixing between a quark (antiquark) and a hole of thermally excited antiquarks (quarks), leading to a level repulsion or gap in the resultant physical spectrum. These mixings are understood in terms of the resonant scattering^{19),20)} of the quasi-quarks off the bosons. In particular, owing to the mass of the boson, the level repulsion due to the resonant scattering occurs *twice* on the different points in the energy-momentum plane, leading to the three-peak structure of the spectral function. This is contrasted to the quark spectrum coupled to a massless boson like a gauge boson, where the resonant scattering occurs only at the origin in the energy-momentum plane and then leads to only two peaks as in the spectrum in the

HTL approximation.

Since there may exist bosonic excitations, even apart from gluons, coupled to quarks in the QGP phase,^{4),25),26)} it is plausible that the quark spectrum has a three-peak structure in the QGP phase if the boson has a “mass” of the order of T ; if there exist several bosonic excitations with “masses” around T , the quark spectral function may become a superposition of the three-peak structures with various heights. Although the quark spectral function in QCD is a gauge-dependent quantity, the complex pole of the quark Green function is gauge-invariant. In this sense we expect that the peak structure of the quark spectral function reflects the complex pole of the Green function and will be seen in gauge theories like QCD.

One of interesting examples of the bosonic excitations which may affect the quasi-particle picture of the quarks in the QGP phase is the soft modes associated with the chiral transition;⁴⁾ the chiral soft mode is unique since its effective mass $m_\sigma^*(T)$ may become as light as a few hundred MeV and thus can be eventually the same order as T near T_c of the chiral transition, if the phase transition is second or weakly first order. In fact, it has been shown⁷⁾ that the chiral soft modes give rise to a three-peak structure in the quark spectrum near but above T_c : In Ref. 7), the Nambu-Jona-Lasinio model is employed as a chiral model and the quark spectral function is calculated incorporating the effect of the dynamically generated soft modes into quark propagator. It is noteworthy that although the soft mode obtained in a dynamical model as employed in Ref. 7) is a composite particle with a finite width and not exactly an elementary boson, a clear three-peak structure is realized in the quark spectral function.

It is interesting to investigate the effect of the change of the quark spectrum on various observables in the QGP phase. In particular, it is intriguing to explore the dilepton production rate; since the quasiparticle peaks in the three-peak structure have low sound velocities, there can appear a sharp peak in the dilepton production rate owing to the similar mechanism as the van Hove singularities.²⁷⁾ It is also an interesting subject to consider the property of the mesonic excitation in the QGP phase composed of the quarks having the spectrum obtained in this work.

We remark that the lattice QCD simulation of the quark spectrum will be, of course, preferable, although some works will be involved such as the gauge fixing, making the chiral extrapolation and using dynamical (chiral) fermions to see the effects of the chiral soft modes.

Since the present investigation is based on simple but generic Yukawa models with a massive scalar and vector boson, the results obtained here should apply to various systems at finite T composed of a light fermion and a massive boson, even apart from the QCD matter in the QGP phase. One of them is the excitation spectra of the neutrinos coupled to the weak bosons at high T around the masses of the weak bosons,²⁸⁾ where the investigation is made exclusively in terms of the neutrino quasi-dispersion relations.

In this paper, we have considered only the massless quarks. However, the finite quark mass should affect the formation of the three-peak structure in the quark spectral function. Incorporation of the quark mass effect is also important for describing the chiral transition precisely because the order of the transition and hence the quark

spectrum near the critical point are sensitive to the quark mass. The finite quark mass also leads to a difference between the scalar(vector) and pseudoscalar(axial-vector) boson cases. Such a study²⁹⁾ and the study³⁰⁾ of the quark spectrum at finite density are now under way and will be reported elsewhere.

Acknowledgements

M.K. is grateful to Y. Hidaka and R. D. Pisarski for useful discussions. He also acknowledges L. McLerran and F. Karsch for their interest in this work. T. K. acknowledges B. Muller for valuable comments. Y.N. thanks M. Harada for useful comments. M.K. is supported by Special Postdoctoral Research Program of RIKEN. T.K. is supported by Grant-in-Aid for Scientific Research by Monbu-Kagakusyo (No. 17540250). Y.N. is supported by the 21st Century COE Program of Nagoya University and Grand-in-Aid for Scientific Research by Monbu-Kagakusyo (No. 18740140). This work is supported by the Grant-in-Aid for the 21st Century COE “Center for Diversity and Universality in Physics” of Kyoto University.

Appendix A

— Quark self-energy in the Yukawa model with the scalar coupling —

In this appendix, we summarize the calculation of the quark self-energy in the model with the scalar boson eq. (3·2);

$$\tilde{\Sigma}(\mathbf{p}, i\omega_m) = -g^2 T \sum_n \int \frac{d^3 \mathbf{k}}{(2\pi)^3} \mathcal{G}_0(\mathbf{k}, i\omega_n) \mathcal{D}(\mathbf{p} - \mathbf{k}, i\omega_m - i\omega_n), \quad (\text{A}\cdot1)$$

where

$$\mathcal{G}_0(\mathbf{k}, i\omega_n) = \frac{1}{i\omega_n \gamma^0 - \mathbf{k} \cdot \boldsymbol{\gamma}} = \sum_s \Lambda_s(\mathbf{k}) \gamma^0 \frac{1}{i\omega_n - sE_f}, \quad (\text{A}\cdot2)$$

$$\mathcal{D}(\mathbf{k}, i\nu_n) = \frac{1}{(i\nu_n)^2 - \mathbf{k}^2 - m^2} = \sum_t t \frac{1}{2E_b(i\nu_n - tE_b)} \quad (\text{A}\cdot3)$$

are the free propagators of the quark and the scalar boson, respectively. $\Lambda_{\pm}(\mathbf{k}) = (1 \pm \gamma^0 \boldsymbol{\gamma} \cdot \hat{\mathbf{k}})/2$ are the projection operators onto positive and negative energies, respectively. Substituting eqs.(A·2) and (A·3) into eq. (A·1), we have

$$\tilde{\Sigma}(\mathbf{p}, i\omega_m) = -g^2 \sum_{s,t=\pm} T \sum_n \int \frac{d^3 \mathbf{k}}{(2\pi)^3} \frac{t\Lambda_s(\mathbf{k})\gamma^0}{2E_b} \frac{1}{i\omega_n - sE_f} \cdot \frac{1}{i\omega_m - i\omega_n - tE_b}, \quad (\text{A}\cdot4)$$

with $E_f = |\mathbf{k}|$, $E_b = \sqrt{(\mathbf{p} - \mathbf{k})^2 + m^2}$. Taking the summation of the Matsubara mode n and the analytic continuation $i\omega_m \rightarrow \omega + i\eta$ in eq. (A·4), we obtain the retarded self-energy and its imaginary part;

$$\Sigma^R(\mathbf{p}, \omega) = -g^2 \sum_{s,t=\pm} \int \frac{d^3 \mathbf{k}}{(2\pi)^3} \frac{t\Lambda_s(\mathbf{k})\gamma^0}{2E_b} \frac{f(sE_f) + n(-tE_b)}{\omega - sE_f - tE_b + i\eta}, \quad (\text{A}\cdot5)$$

$$\text{Im}\Sigma^R(\mathbf{p}, \omega) = \pi g^2 \sum_{s,t=\pm} \int \frac{d^3\mathbf{k}}{(2\pi)^3} \frac{t\Lambda_s(\mathbf{k})\gamma^0}{2E_b} \{f(sE_f) + n(-tE_b)\} \delta(\omega - sE_f - tE_b). \quad (\text{A.6})$$

Eqs. (3.3) and eq. (3.6) are obtained by taking the summation s and t in eqs.(A.5) and (A.6), respectively.

We decompose the self-energy with the projection operators into $\Sigma^R(\mathbf{p}, \omega) = \Sigma_+(\mathbf{p}, \omega)\Lambda_+(\mathbf{p})\gamma^0 + \Sigma_-(\mathbf{p}, \omega)\Lambda_-(\mathbf{p})\gamma^0$. The imaginary part of $\Sigma_+(\mathbf{p}, \omega)$ is calculated in the following way,

$$\begin{aligned} \text{Im}\Sigma_+(\mathbf{p}, \omega) &= \frac{1}{2}\text{Tr}[\text{Im}\Sigma^R(\mathbf{p}, \omega)\Lambda_+(\mathbf{p})\gamma^0] \\ &= \pi g^2 \sum_{s,t=\pm} \int \frac{d^3\mathbf{k}}{(2\pi)^3} \frac{1 - s\hat{\mathbf{p}} \cdot \hat{\mathbf{k}}}{4tE_b} \{f(sE_f) + n(-tE_b)\} \delta(\omega - sE_f - tE_b) \end{aligned} \quad (\text{A.7})$$

$$\begin{aligned} &= -\frac{g^2}{32\pi\mathbf{p}^2} \sum_{s,t=\pm} st \int dE_f \int_{e_-}^{e_+} dE_b [(|\mathbf{p}| - sE_f)^2 - E_b^2 + m^2] \\ &\quad \times \{f(sE_f) + n(-tE_b)\} \delta(\omega - sE_f - tE_b) \\ &= -\frac{g^2}{32\pi\mathbf{p}^2} \sum_{s,t=\pm} st \int dE_f [(|\mathbf{p}| + \omega - 2E_f)(|\mathbf{p}| - \omega) + m^2] \\ &\quad \times \{f(sE_f) + n(sE_f - \omega)\} \int_{e_-}^{e_+} dE_b \delta(\omega - sE_f - tE_b), \end{aligned} \quad (\text{A.8})$$

where in the third equality we have used the relations

$$\hat{\mathbf{p}} \cdot \hat{\mathbf{k}} = \frac{\mathbf{p}^2 + E_f^2 - E_b^2 + m^2}{2|\mathbf{p}|E_f}, \quad (\text{A.9})$$

$$\int \frac{d^3\mathbf{k}}{(2\pi)^3} = \frac{1}{4\pi^2|\mathbf{p}|} \int dE_f E_f \int_{e_-}^{e_+} dE_b E_b, \quad (\text{A.10})$$

with $e_{\pm} = \sqrt{(|\mathbf{p}| \pm E_f)^2 + m^2}$.

In the time-like region, one of the four terms in eq. (A.8) takes a finite value (See, Fig. 2). After some algebra, it is found that all these terms in the time-like region are reduced to the following simple form:

$$\begin{aligned} \text{Im}\Sigma_+(\mathbf{p}, \omega) &= -\frac{g^2}{32\pi\mathbf{p}^2} \int_{E_f^+}^{E_f^-} dE_f [(|\mathbf{p}| + \omega - 2E_f)(|\mathbf{p}| - \omega) + m^2] \\ &\quad \times \{f(sE_f) + n(sE_f - \omega)\}, \end{aligned} \quad (\text{A.11})$$

with

$$E_f^{\pm} = \frac{\omega^2 - \mathbf{p}^2 - m^2}{2(\omega \pm |\mathbf{p}|)}. \quad (\text{A.12})$$

In the space-like region, two terms corresponding to (II) and (III) in Fig. 3 take finite values, and eq. (A.8) is calculated to be

$$\begin{aligned}
\text{Im}\Sigma_+(\mathbf{p}, \omega) &= -\frac{g^2}{32\pi\mathbf{p}^2} \left[\int_{E_f^+}^{-\infty} dE_f - \int_{\infty}^{E_f^-} dE_f \right] [(|\mathbf{p}| + \omega - 2E_f)(|\mathbf{p}| - \omega) + m^2] \\
&\quad \times \{f(E_f) + n(E_f - \omega)\} \\
&= -\frac{g^2}{32\pi\mathbf{p}^2} \left[\int_{E_f^+}^{E_f^-} dE_f - \int_{-\infty}^{\infty} dE_f \right] [(|\mathbf{p}| + \omega - 2E_f)(|\mathbf{p}| - \omega) + m^2] \\
&\quad \times \{f(E_f) + n(E_f - \omega)\} \\
&= -\frac{g^2}{32\pi\mathbf{p}^2} \int_{E_f^+}^{E_f^-} dE_f [(|\mathbf{p}| + \omega - 2E_f)(|\mathbf{p}| - \omega) + m^2] \{f(E_f) + n(E_f - \omega)\} \\
&\quad - \frac{\pi g^2 T^2}{32} \frac{|\mathbf{p}| - \omega}{\mathbf{p}^2} - \frac{g^2}{32\pi} \frac{\omega[|\mathbf{p}|(|\mathbf{p}| - \omega) + m^2]}{\mathbf{p}^2}, \tag{A.13}
\end{aligned}$$

where we used the integral formulae

$$\int_{-\infty}^{\infty} d\epsilon [f(\epsilon) + n(\epsilon - \omega)] = -\omega, \tag{A.14}$$

$$\int_{-\infty}^{\infty} d\epsilon \epsilon [f(\epsilon) - n(\epsilon - \omega)] = \frac{\pi^2 T^2}{2} + \frac{\omega^2}{2}. \tag{A.15}$$

Equations (A.11) and (A.13) are combined to

$$\begin{aligned}
\text{Im}\Sigma_+(\mathbf{p}, \omega) &= -\frac{g^2}{32\pi\mathbf{p}^2} \int_{E_f^+}^{E_f^-} dE_f [(|\mathbf{p}| + \omega - 2E_f)(|\mathbf{p}| - \omega) + m^2] \{f(E_f) + n(E_f - \omega)\} \\
&\quad - \left\{ \frac{\pi g^2 T^2}{32} \frac{|\mathbf{p}| - \omega}{\mathbf{p}^2} + \frac{g^2}{32\pi} \frac{\omega[|\mathbf{p}|(|\mathbf{p}| - \omega) + m^2]}{\mathbf{p}^2} \right\} \theta(\mathbf{p}^2 - \omega^2). \tag{A.16}
\end{aligned}$$

For vanishing momentum $\mathbf{p} = \mathbf{0}$, from eq. (A.7) we obtain,

$$\text{Im}\Sigma_{\pm}(\mathbf{0}, \omega) = -\frac{g^2}{64\pi} \frac{(\omega^2 - m^2)^2}{\omega^3} \left(\coth \frac{\omega^2 + m^2}{4T\omega} + \tanh \frac{\omega^2 - m^2}{4T\omega} \right). \tag{A.17}$$

The T -independent part of $\text{Im}\Sigma_+(\mathbf{p}, \omega)$ is given by the $T = 0$ limit of eq. (A.16). In this case one can perform the integral in eq. (A.16) analytically and obtains

$$\text{Im}\Sigma_+(\mathbf{p}, \omega)_{T=0} = -\frac{g^2}{32\pi} (\omega - |\mathbf{p}|) \frac{(P^2 - m^2)^2}{P^4} \text{sgn}(\omega) \theta(P^2 - m^2), \tag{A.18}$$

with $P^2 = \omega^2 - \mathbf{p}^2$.

The T -dependent part $\text{Im}\Sigma_+^R(\mathbf{p}, \omega)_{T \neq 0}$ is obtained by a replacement of the distribution function in the curly bracket in eq. (A.8) as

$$f(E_f) + n(\omega - E_f) \rightarrow n(\omega - E_f) + f(E_f) + \epsilon(\omega) \theta(P^2 - m^2). \tag{A.19}$$

Appendix B

— Quark self-energy in the Yukawa model with the vector coupling —

The self-energy of the quark in a Yukawa model with a massive vector boson is given by eq. (4.3);

$$\tilde{\Sigma}(\mathbf{p}, i\omega_m) = -g^2 T \sum_n \int \frac{d^3 \mathbf{k}}{(2\pi)^3} \gamma^\mu \mathcal{G}_0(\mathbf{k}, i\omega_n) \gamma^\nu \mathcal{D}_{\mu\nu}(\mathbf{p} - \mathbf{k}, i\omega_m - i\omega_n), \quad (\text{B.1})$$

with the Proca propagator $\mathcal{D}_{\mu\nu}$ defined in eq. (4.4). Taking the summation of the Matsubara mode n and the analytic continuation $i\omega_m \rightarrow \omega + i\eta$, the retarded self-energy $\Sigma^R(\mathbf{p}, \omega)$ is obtained as eq. (4.5) and the imaginary part is given by

$$\begin{aligned} \text{Im}\Sigma^R(\mathbf{p}, \omega) &= -\pi g^2 \sum_{s,t=\pm} t \int \frac{d^3 \mathbf{k}}{(2\pi)^3} \frac{\gamma^\mu \Lambda_s(\mathbf{k}) \gamma^0 \gamma^\nu}{2E_b} \left(g_{\mu\nu} - \frac{q_\mu q_\nu}{m^2} \right) \\ &\quad \times \{f(sE_f) + n(-tE_b)\} \delta(\omega - sE_f - tE_b), \end{aligned} \quad (\text{B.2})$$

with $E_f = |\mathbf{k}|$, $E_b = \sqrt{(\mathbf{p} - \mathbf{k})^2 + m^2}$ and $q_\mu = (tE_b, \mathbf{p} - \mathbf{k})$. The quark sector of eq. (B.2) is calculated to give

$$\begin{aligned} \text{Im}\Sigma_+(\mathbf{p}, \omega) &= \text{Tr} [\text{Im}\Sigma^R(\mathbf{p}, \omega) \Lambda_+(\mathbf{p}) \gamma^0] \\ &= \pi g^2 \sum_{s,t=\pm} t \int \frac{d^3 \mathbf{k}}{(2\pi)^3} \frac{t}{2E_b} \left[\frac{(tE_b - s\hat{\mathbf{k}} \cdot \mathbf{q})(tE_b - \hat{\mathbf{p}} \cdot \mathbf{q})}{m^2} - \frac{1 - s\hat{\mathbf{k}} \cdot \hat{\mathbf{p}}}{2} \right] \\ &\quad \times \{f(sE_f) + n(-tE_b)\} \delta(\omega - sE_f - tE_b) \\ &= \frac{g^2}{32\pi \mathbf{p}^2 m^2} \sum_{s,t=\pm} st \int dE_f [(\mathbf{p}^2 - \omega^2 + m^2) ((|\mathbf{p}| - \omega)^2 - 2m^2) \\ &\quad + 2sE_f(\mathbf{p}^2 - \omega^2 + 2m^2)(|\mathbf{p}| - \omega)] \int_{E_f^-}^{E_f^+} dE_b \delta(\omega - sE_f - tE_b) \\ &= -\frac{g^2}{32\pi \mathbf{p}^2 m^2} \int_{E_f^+}^{E_f^-} d\epsilon [-(P^2 - m^2) \{ (|\mathbf{p}| - \omega)^2 - 2m^2 \} \\ &\quad + 2\epsilon(\omega - |\mathbf{p}|)(P^2 - 2m^2)] \{ f(\epsilon) + n(\epsilon - \omega) \} \\ &\quad - \frac{g^2}{32\pi \mathbf{p}^2 m^2} \theta(-P^2) \left\{ (P^2 - 2m^2)(\omega - |\mathbf{p}|) \pi^2 T^2 \right. \\ &\quad \left. + \omega[2m^4 - P^2 \{ |\mathbf{p}|(\omega - |\mathbf{p}|) + m^2 \}] \right\}. \end{aligned} \quad (\text{B.3})$$

where in the third equality we used eqs. (A.9), (A.10) and

$$\hat{\mathbf{k}} \cdot \mathbf{q} = \frac{\mathbf{p}^2 - E_f^2 - E_b^2 + m^2}{2E_f}, \quad \hat{\mathbf{p}} \cdot \mathbf{q} = \frac{\mathbf{p}^2 - E_f^2 + E_b^2 - m^2}{2|\mathbf{p}|}. \quad (\text{B.4})$$

For vanishing momentum $\mathbf{p} = \mathbf{0}$, we have

$$\text{Im}\Sigma_\pm(\mathbf{0}, \omega) = -\frac{g^2}{64\pi} \omega \frac{\omega^2 + 2m^2}{m^2} \frac{(\omega^2 - m^2)^2}{\omega^4} \left(\coth \frac{\omega^2 + m^2}{4T\omega} + \tanh \frac{\omega^2 - m^2}{4T\omega} \right).$$

(B·5)

For the T -independent part which is given by the $T = 0$ limit in eq. (B·3), one can perform the integral in eq. (B·3) analytically and obtains

$$\text{Im}\Sigma_+(\mathbf{p}, \omega)_{T=0} = -\frac{g^2}{32\pi}(\omega - |\mathbf{p}|)\frac{P^2 + 2m^2}{P^2}\frac{(P^2 - m^2)^2}{P^4}\text{sgn}(\omega)\theta(P^2 - m^2), \quad (\text{B}\cdot6)$$

with $P^2 = \omega^2 - \mathbf{p}^2$.

Appendix C

Renormalization of the T -independent part

In this appendix, we perform the renormalization of the T -independent part of the self-energy $\Sigma(\mathbf{p}, \omega)_{T=0}$ in the models in Secs. 3 and 4. Because the imaginary part of $\Sigma^R(\mathbf{p}, \omega)_{T=0}$ in both the models is free from ultraviolet divergence as shown in appendices A and B, the renormalization is needed for the real part only. The T -independent part has the Lorentz covariance. To calculate $\Sigma(\mathbf{p}, \omega)_{T=0}$ by keeping this symmetry explicitly, we employ the self-energy in the Feynman propagator Σ^F instead of the retarded one Σ^R . Once the renormalized self-energy in the Feynman propagator is derived, the corresponding retarded one is readily obtained. In the following, we omit the subscript of the self-energy, $\Sigma^F \equiv \Sigma_{T=0}^F$.

Because of the Lorentz invariance, the self-energy is of the following form;

$$\Sigma^F(\mathbf{p}, \omega) = \not{p}\Sigma_1^F(P^2) + \Sigma_2^F(P^2), \quad (\text{C}\cdot1)$$

with $p^\mu = (\omega, \mathbf{p})$. For the self-energy used in Secs.3 and 4, $\Sigma_2(P^2)$ vanishes.

We regularize the real part of the self-energy with the subtracted dispersion relation, which is much more convenient than the others, e.g., the Pauli-Villars or the dimensional regularization; we have confirmed that these regularizations give the same result in our models. The subtracted dispersion relation is written as

$$\text{Re}\Sigma_1^F(P^2) = \sum_{l=0}^{n-1} \frac{(P^2 - \alpha)^l}{l!} c_l + \frac{(P^2 - \alpha)^n}{\pi} \text{P} \int_{s_{\text{thr}}}^{\infty} ds \frac{\text{Im}\Sigma_1^F(s)}{(s - P^2)(s - \alpha)^n}, \quad (\text{C}\cdot2)$$

where α denotes the subtraction point or the renormalization point, and s_{thr} denotes the threshold which is given by $s_{\text{thr}} = m^2$ in our case. The parameters c_l are the subtraction constants which are to be determined by the renormalization condition. Equation (C·2) is valid for $\alpha < s$.

C.1. Renormalization in the Yukawa model with the scalar coupling

From Appendix. A, the imaginary part of $\Sigma_1^F(P^2)$ reads

$$\text{Im}\Sigma_1^F(P^2) = -\frac{g^2}{32\pi} \frac{(P^2 - m^2)^2}{P^4} \theta(P^2 - m^2). \quad (\text{C}\cdot3)$$

For the real part of Σ_1^F , we use the subtracted dispersion relation eq. (C·2) for $n = 1$ to regularize the ultraviolet divergence. We impose the on-shell renormalization

condition, $\Sigma_1^F(P^2 = \alpha) = 0$ and $\alpha = 0$. From eq. (C.3), we have $\text{Im}\Sigma_1^F(P^2 = 0) = 0$. The renormalized real part is then given by

$$\begin{aligned}\text{Re}\Sigma_1^F(P^2) &= \frac{P^2}{\pi} \text{P} \int_{m^2}^{\infty} ds \frac{\text{Im}\Sigma_1^F(s)}{s(s - P^2)} \\ &= \frac{g^2}{32\pi^2} \left\{ \frac{(P^2 - m^2)^2}{P^4} \log \left| \frac{P^2 - m^2}{m^2} \right| - \frac{3}{2} + 2\frac{m^2}{P^2} \right\}.\end{aligned}\quad (\text{C.4})$$

The retarded self-energy $\Sigma^R(\mathbf{p}, \omega)$ is given by $\text{Re}\Sigma^R(\mathbf{p}, \omega) = \text{Re}\Sigma^F(P^2)$ and $\text{Im}\Sigma^R(\mathbf{p}, \omega) = \epsilon(\omega)\text{Im}\Sigma^F(P^2)$;

$$\begin{aligned}\Sigma^R(\mathbf{p}, \omega) &= \frac{g^2}{32\pi^2} \not{p} \left\{ \frac{(P^2 - m^2)^2}{P^4} \log \left| \frac{P^2 - m^2}{m^2} \right| - \frac{3}{2} + 2\frac{m^2}{P^2} \right\} \\ &\quad - i \frac{g^2}{32\pi} \not{p} \frac{(P^2 - m^2)^2}{P^4} \epsilon(\omega) \theta(P^2 - m^2).\end{aligned}\quad (\text{C.5})$$

C.2. Renormalization in the Yukawa model with the vector coupling

From eq. (B.6), the imaginary part of the self-energy Σ_1^F reads

$$\text{Im}\Sigma_1^F(P^2) = -\frac{g^2}{32\pi} \frac{P^2 + 2m^2}{m^2} \frac{(P^2 - m^2)^2}{P^4} \theta(P^2 - m^2).\quad (\text{C.6})$$

To renormalize the real part, we need the subtracted dispersion relation eq. (C.2) for $n = 2$.

$$\begin{aligned}\text{Re}\Sigma_1^F(P^2) &= c_0 + c_1 P^2 + \frac{P^4}{\pi} \text{P} \int_{m^2}^{\infty} ds \frac{\text{Im}\Sigma_1^F(s)}{s^2(s - P^2)} \\ &= c_0 + c_1 P^2 \\ &\quad + \frac{g^2}{32\pi^2} \left\{ \frac{P^2 + 2m^2}{m^2} \frac{(P^2 - m^2)^2}{P^4} \log \left| \frac{P^2 - m^2}{m^2} \right| - \frac{5}{6} \frac{P^2}{m^2} - 2 + 2\frac{m^2}{P^2} \right\}.\end{aligned}\quad (\text{C.7})$$

where we set $\alpha = 0$. One finds that the on-shell renormalization condition $\Sigma_1^F(P^2 = 0) = 0$ is not enough to remove all the divergent parts. Here we impose an additional condition, $c_1 = 0$, to give the renormalized self-energy

$$\text{Re}\Sigma_1^F(P^2) = \frac{g^2}{32\pi^2} \left\{ \frac{P^2 + 2m^2}{m^2} \frac{(P^2 - m^2)^2}{P^4} \log \left| \frac{P^2 - m^2}{m^2} \right| - \frac{5}{6} \frac{P^2}{m^2} - 2 + 2\frac{m^2}{P^2} \right\}.\quad (\text{C.8})$$

Therefore the renormalized retarded self-energy is given by

$$\begin{aligned}\Sigma_1^R(P^2) &= \frac{g^2}{32\pi^2} \left\{ \frac{P^2 + 2m^2}{m^2} \frac{(P^2 - m^2)^2}{P^4} \log \left| \frac{P^2 - m^2}{m^2} \right| - \frac{5}{6} \frac{P^2}{m^2} - 2 + 2\frac{m^2}{P^2} \right\} \\ &\quad - i \frac{g^2}{32\pi} \frac{P^2 + 2m^2}{m^2} \frac{(P^2 - m^2)^2}{P^4} \text{sgn}(\omega) \theta(P^2 - m^2).\end{aligned}\quad (\text{C.9})$$

Appendix D

— Limiting behavior of $\Sigma^R(\mathbf{p}, \omega)$ in the Yukawa model with the vector coupling —

In Section 4, we have shown that the thermal mass of the quark coupled with the vector boson in the Proca formalism approaches $\omega = \sqrt{6}m$ in the high T limit, where m is the mass of the vector boson. In this section, we prove this limiting behavior. Since we are interested in the thermal mass, we only consider the quark propagator at vanishing momentum and omit the subscript and the argument of the momentum in the self-energy, $\Sigma_{\pm}(\mathbf{p} = 0, \omega) \equiv \Sigma(\omega)$, in the following.

Let us first derive the analytic form of $\text{Re}\Sigma(\omega)$ in the high T limit, where the T -independent part is negligible. Thus we consider the T -dependent part $\text{Re}\Sigma(\omega)_{T \neq 0}$ which is calculated from the unsubtracted dispersion relation eq. (3.5),

$$\text{Re}\Sigma(\omega)_{T \neq 0} = -\frac{1}{\pi} P \int_{-\infty}^{\infty} dz \frac{\text{Im}\Sigma(z)_{T \neq 0}}{\omega - z} = -\frac{2\omega}{\pi} P \int_0^{\infty} dz \frac{\text{Im}\Sigma(z)_{T \neq 0}}{\omega^2 - z^2}. \quad (\text{D.1})$$

In the second equality, we used the relation $\text{Im}\Sigma(\omega) = \text{Im}\Sigma(-\omega)$ which is valid for the massless quark at vanishing momentum. Here, $\text{Im}\Sigma(\omega)_{T \neq 0}$ is given by

$$\begin{aligned} \text{Im}\Sigma(\omega)_{T \neq 0} &= -\frac{g^2}{64\pi} \frac{\omega^2 + 2m^2}{m^2} \frac{(\omega^2 - m^2)^2}{\omega^3} \\ &\times \left(\coth \frac{\omega^2 + m^2}{4T\omega} + \tanh \frac{\omega^2 - m^2}{4T\omega} - 2\theta(\omega^2 - m^2) \right). \end{aligned} \quad (\text{D.2})$$

Substituting eq. (D.2) into eq. (D.1), we have the following from:

$$\text{Re}\Sigma(\omega)_{T \neq 0} = \frac{\omega g^2}{32\pi^2} (I_1(\omega) + I_2(\omega)), \quad (\text{D.3})$$

$$\begin{aligned} I_1(\omega) &\equiv P \int_0^m dz \frac{1}{\omega^2 - z^2} \frac{z^2 + 2m^2}{m^2} \frac{(z^2 - m^2)^2}{z^3} \left[\coth \frac{z^2 + m^2}{4Tz} - \tanh \frac{z^2 - m^2}{4Tz} \right] \\ &= \left(\frac{T}{\omega} \right)^2 \int_0^{1/\alpha} \frac{dx}{1 - (\alpha\beta x)^2} \frac{(2 + \alpha^2 x^2)(1 - \alpha^2 x^2)^2}{x^3} \\ &\quad \times \left[\coth \left(\frac{1}{4x} + \frac{\alpha^2 x}{4} \right) - \tanh \left(\frac{1}{4x} - \frac{\alpha^2 x}{4} \right) \right], \end{aligned} \quad (\text{D.4})$$

$$\begin{aligned} I_2(\omega) &\equiv P \int_m^{\infty} dz \frac{1}{\omega^2 - z^2} \frac{z^2 + 2m^2}{m^2} \frac{(z^2 - m^2)^2}{z^3} \left[\coth \frac{z^2 + m^2}{4Tz} - \tanh \frac{z^2 - m^2}{4Tz} - 2 \right] \\ &= -\left(\frac{T}{m} \right)^2 \int_0^{1/\alpha} \frac{dy}{1 - \alpha^2 y^2/\beta^2} \frac{(1 + 2\alpha^2 y^2)(1 - \alpha^2 y^2)^2}{y^3} \\ &\quad \times \left[\coth \left(\frac{1}{4y} + \frac{\alpha^2 y}{4} \right) + \tanh \left(\frac{1}{4y} - \frac{\alpha^2 y}{4} \right) - 2 \right], \end{aligned} \quad (\text{D.5})$$

with $\alpha = m/T$, $\beta = m/\omega$, $x = z/(m\alpha)$ and $y = m/(\alpha z)$.

In the high T limit ($\alpha \rightarrow 0$), the asymptotic form of I_1 and I_2 is given by

$$\begin{aligned} I_1(\omega) &\rightarrow 2 \left(\frac{T}{\omega} \right)^2 \int_0^\infty \frac{dx}{x^3} \left[\coth \left(\frac{1}{4x} \right) - \tanh \left(\frac{1}{4x} \right) \right] \\ &= 4 \left(\frac{T}{\omega} \right)^2 \int_0^\infty dx x \left[\frac{1}{\exp(x/2) - 1} + \frac{1}{\exp(x/2) + 1} \right] \\ &= \frac{4\pi^2 T^2}{\omega^2}, \end{aligned} \quad (\text{D}\cdot6)$$

$$\begin{aligned} I_2(\omega) &\rightarrow - \left(\frac{T}{m} \right)^2 \int_0^\infty \frac{dy}{y^3} \left[\coth \left(\frac{1}{4y} \right) + \tanh \left(\frac{1}{4y} \right) - 2 \right] \\ &= -2 \left(\frac{T}{m} \right)^2 \int_0^\infty dy y \left[\frac{1}{\exp(y/2) - 1} - \frac{1}{\exp(y/2) + 1} \right] \\ &= -\frac{2\pi^2 T^2}{3m^2}. \end{aligned} \quad (\text{D}\cdot7)$$

We have confirmed that the correction terms due to the finite α are $O(\alpha \ln(1/\alpha))$. Therefore the self-energy in the high T limit is given by

$$\lim_{T \rightarrow 0} \text{Re}\Sigma(\omega) = \frac{g^2 T^2}{8} \left(\frac{1}{\omega} - \frac{\omega}{6m^2} \right). \quad (\text{D}\cdot8)$$

In this case the quasi-dispersion relation is given by the solution of the equation $\omega - \text{Re}\Sigma(\omega) \approx -\text{Re}\Sigma(\omega) = 0$, i.e., the zero of $\text{Re}\Sigma(\omega)$. Therefore the energy $\omega = \sqrt{6}m$ gives the thermal mass in the high T limit in this model.

References

- 1) I. Arsene *et al.* [BRAHMS Collaboration], Nucl. Phys. A **757** (2005), 1. B. B. Back *et al.*, Nucl. Phys. A **757** (2005), 28; K. Adcox *et al.* [PHENIX Collaboration], Nucl. Phys. A **757** (2005), 184; J. Adams *et al.* [STAR Collaboration], Nucl. Phys. A **757** (2005), 102.
- 2) T. Umeda, R. Katayama, O. Miyamura and H. Matsufuru, Int. J. Mod. Phys. A **16** (2001), 2215; M. Asakawa and T. Hatsuda, Phys. Rev. Lett. **92** (2004), 012001; S. Datta, F. Karsch, P. Petreczky and I. Wetzorke, Phys. Rev. D **69** (2004), 094507; T. Umeda, K. Nomura and H. Matsufuru, Eur. Phys. J. C **39S1** (2005), 9.
- 3) T. Matsui and H. Satz, Phys. Lett. B **178**, 416 (1986).
- 4) T. Hatsuda and T. Kunihiro, Phys. Lett. B **145** (1984), 7; Phys. Rev. Lett. **55** (1985), 158.
- 5) C. DeTar, Phys. Rev. D **32** (1985), 276.
- 6) R. J. Fries, B. Muller, C. Nonaka and S. A. Bass, Phys. Rev. Lett. **90**, 202303 (2003); Phys. Rev. C **68**, 044902 (2003). V. Greco, C. M. Ko and P. Levai, Phys. Rev. Lett. **90**, 202302 (2003); S. A. Voloshin, Nucl. Phys. A **715**, 379 (2003); D. Molnar and S. A. Voloshin, Phys. Rev. Lett. **91**, 092301 (2003).
- 7) M. Kitazawa, T. Kunihiro and Y. Nemoto, Phys. Lett. B **633** (2006), 269; see also, arXiv:hep-ph/0510381.
- 8) M. Asakawa, S. A. Bass and B. Muller, arXiv:hep-ph/0608270.
- 9) R. D. Pisarski, Phys. Rev. Lett. **63**, 1129 (1989); E. Braaten and R. D. Pisarski, Nucl. Phys. B **337**, 569 (1990); *ibid.*, **B339**, 310 (1990). J. Frenkel and J. C. Taylor, Nucl. Phys. B **334**, 199 (1990).
- 10) See for example, M. Le Bellac, *Thermal Field Theory* (Cambridge University Press, Cambridge, England 1996).

- 11) V. P. Silin, Sov. Phys. JETP **11** (1960), 1136.
- 12) H. A. Weldon, Phys. Rev. D **26** (1982), 1394.
- 13) V. V. Klimov, Sov. J. Nucl. Phys. **33** (1981), 934 [Yad. Fiz. **33** (1981), 1734].
- 14) H. A. Weldon, Phys. Rev. D **40** (1989), 2410; Physica **A 158** (1989), 169; Phys. Rev. D **61** (2000), 036003.
- 15) J. P. Blaizot and J. Y. Ollitrault, Phys. Rev. D **48** (1993), 1390.
- 16) M. Kitazawa, T. Koide, T. Kunihiro and Y. Nemoto, Phys. Rev. D **70** (2004), 056003.
- 17) M. Kitazawa, T. Koide, T. Kunihiro and Y. Nemoto, Prog. Theor. Phys. **114** (2005), 205.
- 18) M. Kitazawa, T. Koide, T. Kunihiro and Y. Nemoto, Phys. Rev. D **65** (2002), 091504.
- 19) M. Kitazawa, T. Kunihiro and Y. Nemoto, Phys. Lett. B **631** (2005), 157.
- 20) B. Janko, J. Mary and K. Levin, Phys. Rev. B **56** (1997), R11407.
- 21) G. Baym, J. P. Blaizot and B. Svetitsky, Phys. Rev. D **46** (1992), 4043.
- 22) H. A. Weldon, Phys. Rev. D **28** (1983), 2007.
- 23) A. Peshier, K. Schertler and M. H. Thoma, Annals Phys. **266** (1998), 162.
- 24) See for example, C. Itzykson and J.B. Zuber, *Quantum Field Theory* (McGraw-Hill, New York, 1980); T. Cheng and L. Li, *Gauge theory of elementary particle physics* (Oxford University Press, New York, 1984).
- 25) E. V. Shuryak and I. Zahed, Phys. Rev. C **70** (2004), 021901; Phys. Rev. D **70** (2004), 054507.
- 26) G. E. Brown, C. H. Lee, M. Rho and E. Shuryak, Nucl. Phys. A **740** (2004), 171; J. Phys. G **30** (2004), S1275; H. J. Park, C. H. Lee and G. E. Brown, Nucl. Phys. A **763** (2005), 197; G. E. Brown, B. A. Gelman and M. Rho, Phys. Rev. Lett. **96** (2006), 132301; G. E. Brown, C. H. Lee and M. Rho, arXiv:nucl-th/0507011.
- 27) E. Braaten, R. D. Pisarski and T. C. Yuan, Phys. Rev. Lett. **64**, 2242 (1990).
- 28) D. Boyanovsky, Phys. Rev. D **72** (2005), 033004.
- 29) K. Mitsutani, M. Kitazawa, T. Kunihiro and Y. Nemoto, in progress.
- 30) M. Kitazawa, T. Kunihiro and Y. Nemoto, in progress.